Measurement, Prediction, and Analysis of the Radio Frequency Electromagnetic Environment Outside and Inside Hospitals

Philip Thomas Vlach, B. Eng. (McGill)

A thesis submitted to the Faculty of Graduate Studies and Research in partial fulfillment of the requirements for the degree of Master of Engineering

Department of Electrical Engineering
McGill University, Montreal

September 1994

ISBN 0-315-99989-6

Spine title (60 characters):

The Radio Frequency Electromagnetic Environment of Hospitals

ABSTRACT

The electromagnetic environment outside and inside five urban hospitals, due to fixed, EXTERNAL TRANSMITTERS (30 - 1000 MHz range), was characterized by measurement. Measured fields generally remained below 130 dBμV/m (3 V/m)., Four computational prediction methods, based on line-of-site free-space propagation, Uniform Geometric Theory of Diffraction, and urban clutter models, were evolved. Fields predicted outside these hospitals were compared to the measured fields. A simple line-of-sight method predicted fields within 20 dB of those measured, thereby easily providing an estimate of the worst-case fields at a hospital. The most complex of these prediction methods estimated field levels to within 10 dB.

Measurements were also used to analyze signal propagation characteristics inside buildings due to INTERNAL SOURCES operating at 433, 861, and 1705 MHz. Cross-floor propagation paths, where multiple floors and walls were traversed, showed fields were independent of the transmitter-receiver separation distance. Signals measured for a separation of one floor were higher than same-floor signal levels.

PRÉCIS

L'environnment électromagnétique produit à l'extérieur et à l'intérieur de cinq hôpitaux urbains par les transmetteurs immobiles EXTERNES opérant entre 30 et 1000 MHz, a été caractérisé par des mesures. Les champs mesurés sont restés, en général, en dessous de 130 dBµV/m (3 V/m). Quatre méthodes computationelles servant à prédire de tels champs électromagnétiques, basées sur des modèles de propagation libre et directe, de l'Uniform Geometric Theory of Diffraction, et de l'obstruction urbaine, ont été développées. Les champs évalués à l'extérieur de ces hôpitaux ont été comparé aux champs mesurés. Une méthode simple, basée sur la propagation directe, a donné des prédictions à 20 dB près, fournissant ainsi facilement une évaluation des pires exemples des champs d'un hôpital. La plus complex de ces méthodes a évalué les niveaux électromagnétiques à 10 dB près.

Autres mesures ont été utilisées pour analyser les caractéristiques de la propagation à l'intérieur des édifices des signaux produits par les sources INTERNES opérant à 433, 861, et 1705 MHz. Les résultats obtenus pour les chemins de la propagation des signaux traversant de multiples étages et murs ont démontré que les champs ont été indépendants de la distance entre le transmetteur et le recepteur. Les niveaux des signaux mesurés pour la separation d'un étage ont été plus hauts qu'au même étage.

ACKNOWLEDGMENTS

The author wishes to express sincere gratitude to the thesis supervisors, Prof. T.J.F. Pavlasek, and Dr. B. Segal, for their untiring support, encouragement, and advice.

Thanks are extended to Philippe Boisvert and Steve Rétfalvi for their invaluable counsel. Thanks also to Messers A. Zafar and L. Farrias at the Royal Victoria Hospital, and to Mr. M. Massaad at St. Mary's Hospital, for their assistance in planning and executing visits to their hospitals.

The participation of Mr. R. Cyr and his colleagues at Industry Canada (formerly the Department of Communications), for assistance with measurements, is gratefully acknowledged.

The author is also grateful to Dr. J. LeBel for providing measurement data for indoor propagation analysis.

The funding of this thesis work by Health and Welfare Canada and, in the final stages, by Bell Mobility/Rogers Cantel is gratefully acknowledged.

TABLE OF CONTENTS

Chapter Page

TABLE OF ILLUSTRATIONS

TABLE OF TABLES

Chapter 1

INTRODUCTION

BACKGROUND

The past several years have been characterized by a dramatic increase in the use of wireless communicators of all types (e.g. cellular phones, pagers, walkie-talkies, telemetry transceivers, emergency radio transmitters used by police, fire, and ambulance). Consequently, the proliferation of mobile wireless communicators, coupled with the growing deployment of fixed radiators, has resulted in an increased spectral and geographic density at radio frequencies (RF), thereby greatly intensifying the general electromagnetic environment (EME).

Concurrently, electrical and electronic devices have evolved from bulky machines to microprocessor-based devices that, accordingly, are smaller and more complex, intelligent, and sophisticated than ever before. However, the advanced technology of the newer generation of devices has made them more vulnerable to external influence, specifically in the form of undesired electromagnetic coupling to outside signals.

The combination of susceptible microprocessor-controlled devices operating in a higher intensity EME has lead to a substantial increase in the number of reported incidents of electromagnetic interference (EMI) [1-4]. This, in turn, has generated a renewed interest in the issue of electromagnetic compatibility (EMC) between modern radiators (fixed/mobile, periodic/aperiodic) and electrical and electronic devices.

THE MEDICAL ENVIRONMENT

The need for EMC is crucial in medical environments, since EMI effects on critical-care medical equipment may have life-threatening results. Silberberg of the U.S. Food and Drug Administration has catalogued several incidences of medical device malfunction attributable to EMI [1,2]. A cross-section of examples is reprinted below from [1]:

- External defibrillator/pacemaker stopped pacing when ambulance attendant used hand-held transmitter too close to patient. Patient not resuscitated. (March & April 1991)
- Investigational implantable defribrillator output inappropriate shocks when user operated radio-controlled model car. (Sept. 1992)
- Infusion pump changed rate when cellular phone placed on instrument stand. (Aug. 1992)
- A fetal heart beat detector picked up radio and CB broadcasts and static instead of heart beats. (July 1980)

Such malfunctions might have been prevented by adherence to appropriate EMC standards. However, critical-care medical equipment is only partly regulated for emission and susceptibility requirements. All of the susceptibility regulations are as yet voluntary or otherwise non-applicable (e.g. FDA MDS 201 00041979) [2,5]. The subject of standards and regulations, although a major issue, is not considered in this thesis. It is, however, noted that the issue of standards and regulations is evolving rapidly, and represents a substantial motivating force for the type of research reported in this thesis.

As health care enters a new era characterized by an emphasis on convalescence in ancillary facilities (especially home-care), the implications of medical device malfunction become especially grave. Occasionally, home users are not completely familiar with the operation of a medical device, particularly when it does not seem to function properly. This is because home-care involves treatment in a non-controlled atmosphere where trained health-care providers are not available, which could have serious consequences. Medical devices will be brought into environments where the ambient EME is unknown, thus potentially exposing patients to risks caused by EMI. In order to assess the broad issue of EMI hazards associated with treatment in ancillary facilities, it is first necessary to examine the comparatively controlled environment within hospitals.

Focus of the Thesis

In trying to achieve the long term objective of an harmonious coexistence in hospitals between critical-care medical equipment and modern radiators, the first step is to characterize the electromagnetic environment of a hospital in order to assess the potential risk of electromagnetic interference. Both the inside and outside EMEs should be considered since they are inextricably linked to one another.

Knowledge of the EME of hospitals provides information for the development of susceptibility requirements for the safe operation of medical equipment in a hospital, as well as assisting in the maintenance of equipment currently in circulation. Furthermore, such knowledge should be used in the design of future generations of medical devices to ensure electromagnetic compatibility.

Critical-care medical equipment in hospitals operates in an electromagnetic environment, referred to as the *inside* EME, that is produced by both *internal* and *external* sources. The *inside* EME due to *external* sources is a function of (i) the EME *outside* due to *external* sources, and (ii) signal penetration from *outside* to *inside*.

Hospitals' electromagnetic environments can be characterized through measurement, but it is both practically and economically unfeasible to measure the EME at every hospital. Thus, it would be invaluable to have a method to estimate a hospital's EME which is simple to apply and sufficiently accurate to be meaningful. Unlike field prediction methods utilized in determining propagation performance for telecommunication systems, such as cellular telephone systems, or point-to-point systems, an EME prediction method for EMC hazard identification does not require a high degree of accuracy.

The range for EME considerations is vast, encompassing the entire known EM spectrum for time harmonic sources and aperiodic phenomena (EM pulses, electrostatic discharge (ESD), lightning). The present thesis will limit itself mainly to the 30 - 1000 MHz range which, however, covers the bulk of fixed radiators such as FM radio, television, and mobile sources.

Therefore, this thesis aims to achieve the following:

(1) To give an overview of the ambient (combined internal and external) electromagnetic environment due to known, fixed, external sources at five Montreal area hospitals. Measurements and predictions of the EME at each hospital will be presented and analyzed;

(2) To examine three additional methods (based on different propagation modelling) for estimating the outside EME due to the highest power, fixed, external sources;

(3) To examine the inside EME, due to internal sources, through an analysis of indoor signal propagation at three frequencies.

THESIS STRUCTURE

The thesis will be in two parts consisting of five chapters.

Part one of the thesis, comprising chapters two through five, will characterize the outside and inside electromagnetic environments of a hospital arising from external, fixed radiators, through measurement and prediction.

In particular, chapter two will present the measured ambient electromagnetic environments of five Montreal area hospitals. Maximum, minimum, and average field levels for each hospital will be shown for frequencies between 30 MHz and

1000 MHz. These measurements will include both outside and inside fields produced by external sources.

Chapters three, four, and five will deal with the development of computational field prediction methods from propagation models [6]. These methods are intended to allow the meaningful estimation of the EME <u>outside</u> a hospital due to fixed, external sources.

Specifically, chapter three will present the results of field predictions made using a simple line-of-sight (LOS). Predictions will be made for all known, fixed, external sources. The LOS predicted fields will be compared to the outside and inside measured fields. The comparison with the inside fields will provide an estimate of the attenuation the field experiences in penetrating into the building at different locations.

Chapter four will introduce a hybrid prediction method for outside fields arising from the highest power, fixed, external sources. A comparison to fields measured outside hospitals will be made in an attempt to objectively assess the performance of this method relative to the LOS method.

In chapter five, the methods of both chapters three and four will be modified by introducing a frequency dependence for the receiving antenna. The prediction methods of chapters three, four, and five will be compared to one another, and to the measured external fields.

Part two of the thesis (chapter six), will deal with indoor signal propagation due to internal sources as a preliminary step to characterizing the effects internal sources have on the electromagnetic environment inside a hospital.

Chapter six will present signal measurements at 433, 861, and 1705 MHz, inside a typical multistory ferro-concrete building (similar to most hospitals). The signals were produced by a source inside the building to evaluate the inside EME due to internal sources. The measured fields will be analyzed to show the effects of signal propagation when the transmitter and the receiver are on the same floor, and when they are separated by one to nine floors.

Chapter seven will summarize the principal findings and suggest areas of future work.

Appendix A will present charts allowing a quick, approximate, graphical evaluation of predicted fields using two line-of-sight methods. Included will be explanations for their use and illustrative examples.

Appendix B will provide a list of the abbreviations used in the thesis.

A list of the books, journal articles, and conference papers cited in the thesis will be provided in "References".

A bibliography of books, journal articles, and conference papers used by the author, but not cited in the thesis, will provide a ready reference list.

PART I: The EME due to External Sources

Chapter 2

FIELD MEASUREMENTS

GENERAL

In an attempt to characterize the electromagnetic environment at hospitals, measurements were made in several locations inside and outside five Montreal area hospitals over the 30 MHz to 1000 MHz range with particular attention to the fields generated by known, fixed, external transmitters. The measurement sites inside the hospitals targeted current and planned critical-care areas, and areas where malfunctions had been previously reported. Exterior measurements were typically made near main entrances to the hospitals. Time constraints allowed only, on average, seven survey sites to be visited per day at each hospital.

The five hospitals surveyed were teaching hospitals of McGill University, four of which are tertiary care centres. An earlier study [3,7] has reported measurements at three of these. The current study surveyed the two hospitals not previously surveyed, and combines the data for all five hospitals. Thus the existing database of measurements was enlarged so that the EMI problem might be better understood.

As the following section suggests, these surveys are time consuming, requiring complex and costly equipment, and trained specialists. Such surveys, therefore, constitute a major activity of planning, execution, and analysis, which is difficult to implement on an extensive scale.

METHODS

Measurements were performed by the Department of Communications (DoC), now Industry Canada, using industry standard techniques. Methods were identical to those reported by Boisvert [7]. The 30 MHz to 1000 MHz range was scanned by an automated system composed of a spectrum analyzer, model A7550 from IFR Systems, connected to a laptop computer. Two measurement antennas were used: (1) a folding biconical antenna, model SAS-200/542 (A.H. Systems), for the 30 MHz to 300 MHz range, and (2) a printed circuit board antenna, model 91597-2 (RI-FI Measuring Equipment), for the 300 MHz to 1000 MHz range.

The 30 - 1000 MHz range was divided into 39 subranges:

- 2 100 MHz subranges in the 200 - 400 MHz band,
- 2 10 MHz subranges in the 30 - 50 MHz band,
- 6 10 MHz subranges in the 110 - 170 MHz band,
- 7 10 MHz subranges in the 400 - 470 MHz band,
- 19 10 MHz subranges in the 800 - 990 MHz band,
- 1 subrange for FM radio,
- 2 subranges for TV transmitters.

The first thirty-six subranges were each swept ten times with resolution bandwidths of 25 kHz (or 250 kHz for subranges of 100 MHz). The maximum signal strength at each <u>active</u> frequency within a bandwidth was retained. Measurements in these thirty-six subranges were made with the antennas vertically polarized [7].

The subrange of Montreal FM radio stations was monitored for ten seconds with the antenna first in the vertical polarization position, then in the horizontal; again the maximum value encountered at each frequency, for each polarization, was retained. However for the purposes of analysis, only the absolute maximum value between the two polarizations, at each frequency, was used.

Television transmissions were divided into two subranges (low and high frequency), and also monitored for ten seconds, but only for a horizontally oriented antenna. Maximum values were retained at each frequency.

For measurements inside hospitals, antennas were placed near windows and, where possible, facing major transmitting towers, so that field levels measured would approximate maximum levels encountered. Note, however, that the hospitals consist of either a large single building, or in many cases, an extended group of buildings covering a considerable geographic area (in some cases the size of a small village).

For measurements outside of the hospitals, the antennas were mounted on a telescoping tower and raised to a height of ten metres. Typically, the tower was positioned near the main entrance to the hospital, and where possible oriented to face the principal cluster of transmitters on Mount Royal. Over one-half hour was needed at each location to complete the measurements in the subranges described above. An average of one outside location and five indoor locations were surveyed in a day.

The data acquired by computer was converted from dBm to dBμV/m as follows [7] :

$$E(dB\mu V/m) = Signal\ Amplitude(dBm) + 107 + Antenna\ Factor + Loss \quad \textbf{(2.1)}$$

A constant of 107 converts dBm to dBμV/m assuming a load of 50 Ω. The antenna specifications supplied by the manufacturer allowed determination of the antenna factor, and the loss due to connecting cables varied as f / (125 x 10^6) for outside measurements, and f / (500 x 10^6) for inside, where f was the measurement frequency.

Boisvert [7] describes the entire measurement process in some detail, as well as experimental equipment under development at McGill. This developmental equipment was also used in the survey of the two additional hospitals, but the data generated by it is not included in this thesis.

The five hospitals surveyed will be designated A, B, C, D, E, where hospitals B, C, D were the three previously surveyed by Boisvert [7]. The current designation differs from that of Boisvert. The designations of the two studies are related as follows:

Current	Boisvert
A	--
B	C
C	A
D	D
E	--

TABLE 2.1: *Relationship of hospital designations between current and Boisvert studies.*

RESULTS and ANALYSIS

The results are presented as spectrographic plots showing the field strengths at a particular measurement site as a function of frequency. Field strengths are plotted in dBμV/m. Figure 2.1 shows the fields measured <u>outside</u> Hospital A.

A graph of this sort was created for each survey site. The dashed lines indicate a voluntary standard showing the maximum allowable limits prescribed by the U.S. Food and Drug Administration in 1979 (Electromagnetic Compatibility Standard for Medical Devices), which required that medical equipment must not exhibit degraded performance when subjected to field strengths of less than, or equal to, 133 dBμV/m between 30 MHz and 470 MHz, and 137 dBμV/m from 470 - 1000 MHz [5,7]. None of the measured fields exceeded this standard by more than 2 dBμV/m. For clarity, only measured signals above the noise floor of the equipment were retained.

Results are also presented in a combined form. That is, in order to obtain an overall indication of the EME at a hospital, the data for <u>all sites</u> in a particular hospital was combined, yielding a mean value, and maximum and minimum deflections from the mean, at each frequency. A graph of the electromagnetic environment at each hospital is shown in figure 2.2. The horizontal line shows the mean, while the vertical lines indicate the extent of the variation of the field throughout the hospital at each frequency. Note that the vertical lines do not correspond to the standard deviation from the mean, but rather show the <u>full</u>

deviation of the fields in each hospital. Again, the dashed lines in each graph indicate the maximum allowable emissions outlined by the U.S. FDA [5].

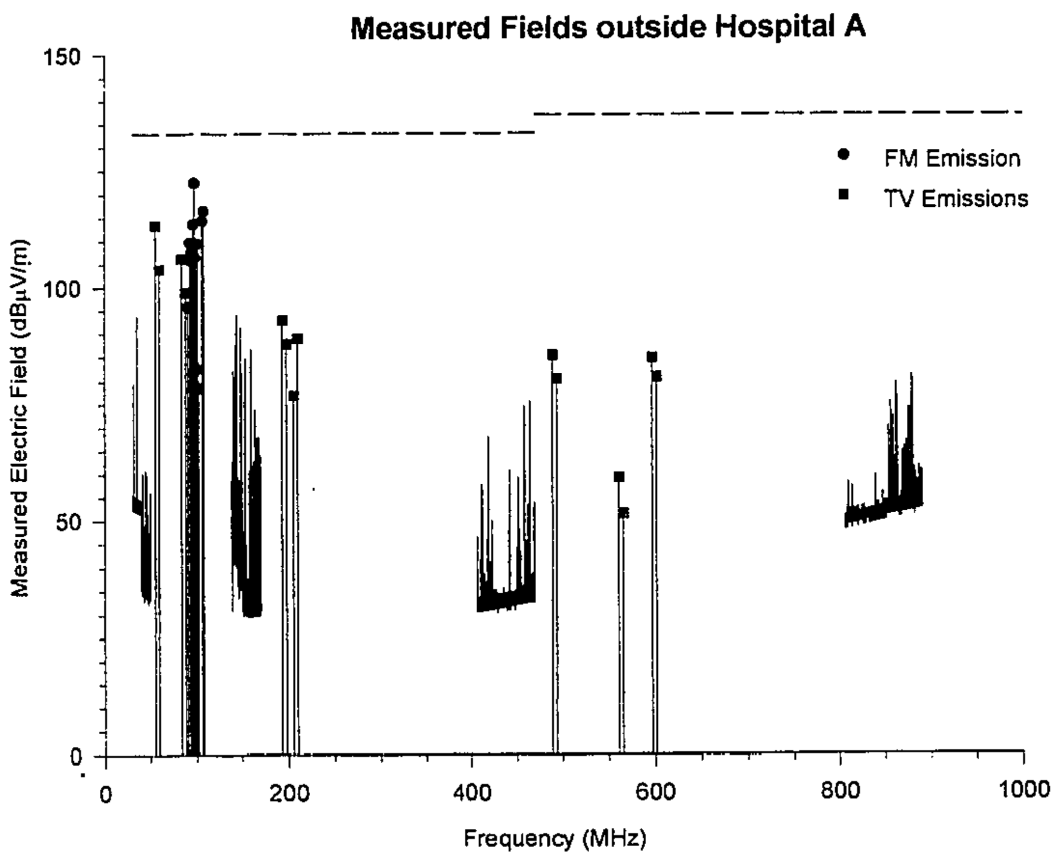

FIGURE 2.1: *Spectrum of fields measured outside Hospital A. In this and all subsequent figures, the dashed lines indicate emission limits prescribed by the U.S. FDA [5].*

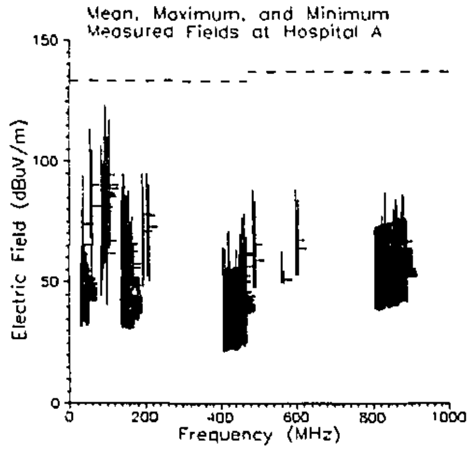

(a) Hospital A

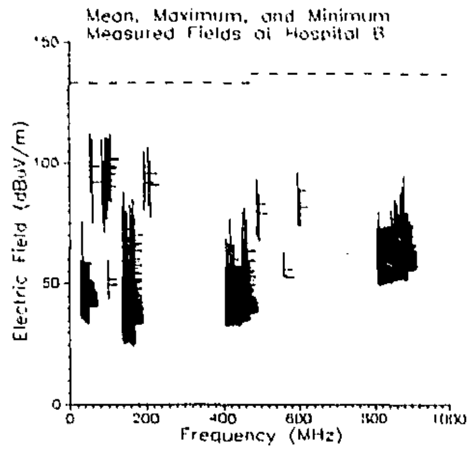

(b) Hospital B

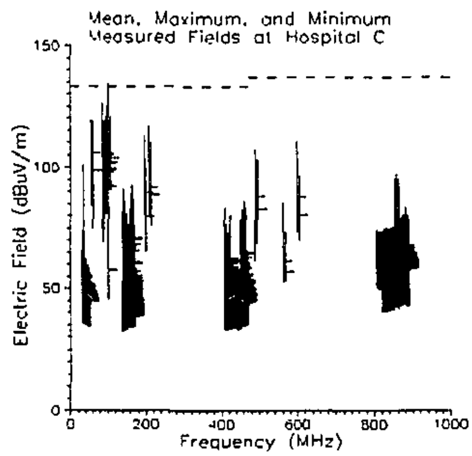

(c) Hospital C

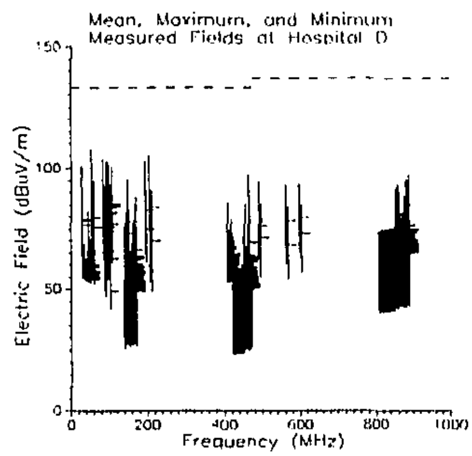

(d) Hospital D

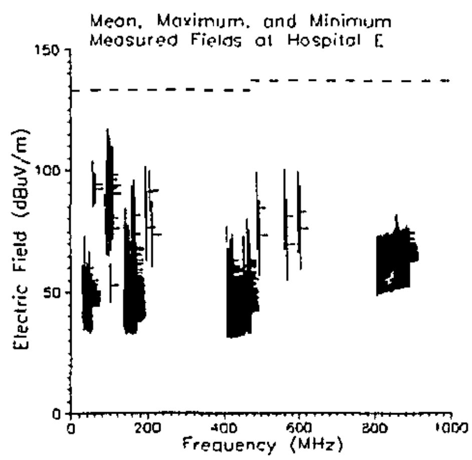

(e) Hospital E

FIGURE 2.2: *Combined internal and external fields measured at five hospitals (mean, maximum, and minimum, in dBμV/m).*

Each graph in figure 2.2 is essentially composed of six distinct frequency bands as follows:

- B-band: 30 - 50 MHz;
- C-band: 138 - 174 MHz;
- D-band: 400 - 470 MHz;
- E-band: 806 - 890 MHz;
- FM band: 88 - 108 MHz;
- TV band: operating frequencies of seven TV stations.

Table 2.2 below shows the average and maximum measured field levels in each band.

Hospital	Average Maximum					
	B-band	C-band	D-band	E-band	FM band	TV band
A	46.09 93.91	40.34 94.16	38.29 77.56	55.09 87.36	83.00 123.20	70.88 113.80
B	45.99 75.90	39.13 88.11	40.21 81.37	56.31 95.13	89.81 112.45	84.77 112.48
C	46.66 100.93	41.61 92.75	45.07 86.37	59.36 97.38	93.40 134.49	85.86 126.34
D	55.84 100.56	51.03 95.16	51.69 97.51	65.68 97.65	76.46 102.71	76.61 107.48
E	48.62 72.90	43.71 95.75	42.82 79.49	62.65 81.36	87.27 116.71	78.55 103.48

TABLE 2.2: *Average and maximum measured field levels in the six active bands ($dB\mu V/m$).*

A comparison of the tabled values (and figure 2.2) clearly demonstrates that the highest average fields regularly occur in the FM and TV bands, while a similar comparison of *maximal* fields in each band reveals the same tendency.

Discussion

Figure 2.1 shows a spectrum of the fields measured at a single survey location outside a hospital. Many measurements of this sort have been combined to produce the graphs in figure 2.2 for each of the five hospitals. A comparison of the average and maximum fields measured in each of the six well defined bands (figure & table 2.2) demonstrates that FM and television transmitters produce the strongest emissions at each hospital, without significantly exceeding the U.S. FDA standard at a particular frequency.

The graphs shown in this chapter presented field strength information at individual, "narrowband" frequency channels for each source transmitter. This type of presentation is especially meaningful when considering tuned receivers (e.g. FM radio, TV, mobile receivers). It should be noted, however, that when considering the susceptibility of electronic medical equipment, which is "broadband" and untuned, a problem arises in assessing the impact of a broadband EM environment such as is shown in figure 2.2. It may be necessary, when dealing with such equipment, to consider the impact of an entire distinct band (as listed in table 2.2), or even the total impact of all six bands. The present study does not pursue this issue but identifies it as important in determining the susceptibility modes of equipment subject to this type of EM environment.

Chapter 3

FIELD PREDICTIONS USING A LINE-OF-SIGHT METHOD

GENERAL

The previous chapter presented a description of the EME of hospitals which may be encountered in large metropolitan cities. The information is based on a large number of lengthy, and costly measurements. It would clearly be desirable to develop a simple, rapid, yet meaningful technique for assessing the EME of a hospital using a computational model based on existing knowledge of the sources. This chapter, as well as chapters four and five, will describe, test, and evaluate several prediction methods based on different propagation models. If such methods of estimating the field levels encountered in hospitals were successful, this approach could serve to reduce the number of measurements that need be made to characterize the EME at hospitals.

The first propagation model, discussed in this chapter, is the free-space line-of-sight (LOS) propagation model, selected since it is the simplest available paradigm to describe signal attenuation due to separation of the field point from the source. Identical predictions were made by Boisvert in 1989 [7]. The results of both studies will be combined, and the predicted fields will be compared to the measured fields outside and inside five hospitals.

METHODS

Field predictions were made for all known, fixed sources in the 30 MHz to 1000 MHz range within about two kilometres of each hospital. Documentation about the location, the radiated field, and the field pattern of every such radiator was obtained from Industry Canada [7]. There were typically two hundred sources at a given hospital.

The line-of-sight propagation model assumes $1/r$ dependence of the field, where r is the line-of-sight transmitter-to-survey site distance, and the transmitter is assumed to be isotropic. Though this method is simple, it serves to establish the usual propagation reference baseline.

Although measurements were made at five hospitals, the results for the <u>outside</u> sites are given for only four. In the case of Hospital C, fields at two sites, C_1 and C_2, were measured. In the case of Hospital E, no results are presented since in the course of analysis it was found that the measurements for the <u>outdoor</u> site were invalid due to equipment failure. This equipment failure, however, was corrected for the <u>indoor</u> measurements at Hospital E.

RESULTS and ANALYSIS

Figure 3.1 shows fields predicted using the line-of-sight model at a location outside Hospital A. Oval symbols indicate the estimated field at each frequency.

These predictions correspond to fields measured at the same outside location, shown in chapter two (figure 2.1).

Similar predictions were made for each survey location, both outside and inside, then combined into comprehensive graphs showing the mean, maximum, and minimum field levels at each frequency throughout an entire hospital. However, no attempt was made to adjust the predicted 'indoor' values for attenuation due to signal penetration into the building.

Figure 3.2 shows one such graph. The horizontal line shows the mean, while the associated vertical lines indicate the maximum and minimum fields predicted at that frequency. The dashed lines at the top of the graph identify the FDA acceptable susceptibility standard for medical devices [5].

Comparison of Measured and Predicted Fields

For every survey location, the measured field was subtracted from the predicted field (**Epredicted - Emeasured**). Again, the results for the sites in a hospital were combined to produce a graph showing the mean, maximum, and minimum differences (figure 3.3). A value below zero indicated that the measured field was stronger than the predicted field.

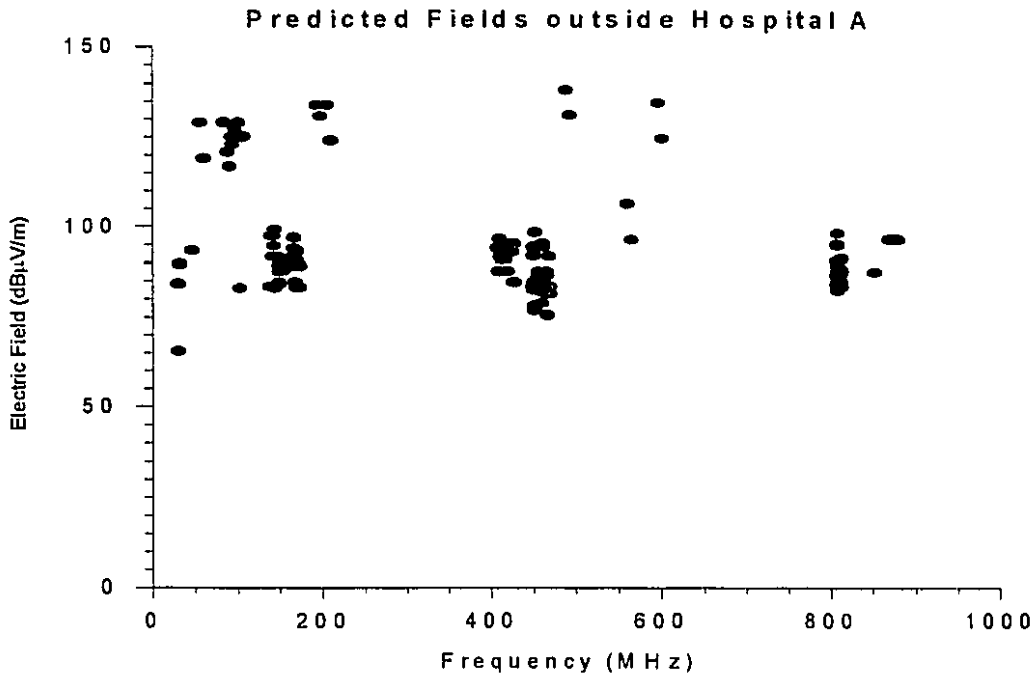

FIGURE 3.1: *Spectrum of fields predicted <u>outside</u> Hospital A.*

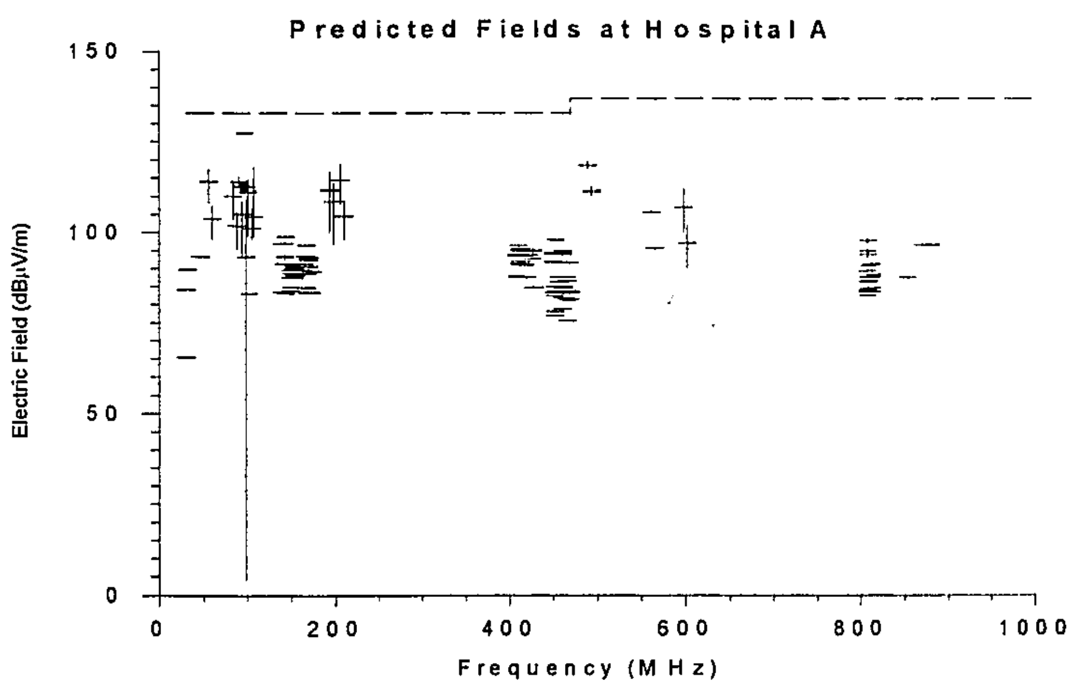

FIGURE 3.2: *Mean, maximum, and minimum fields predicted at Hospital A.*

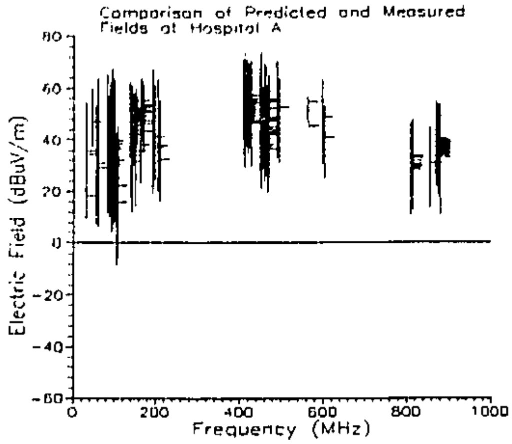

(a) Hospital A

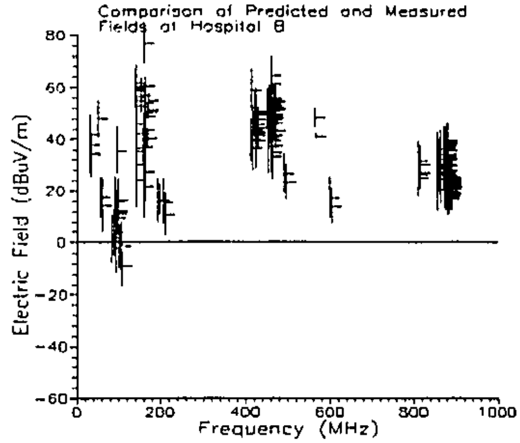

(b) Hospital B

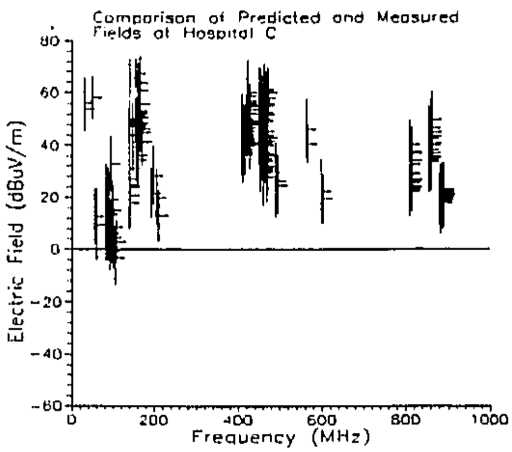

(c) Hospital C

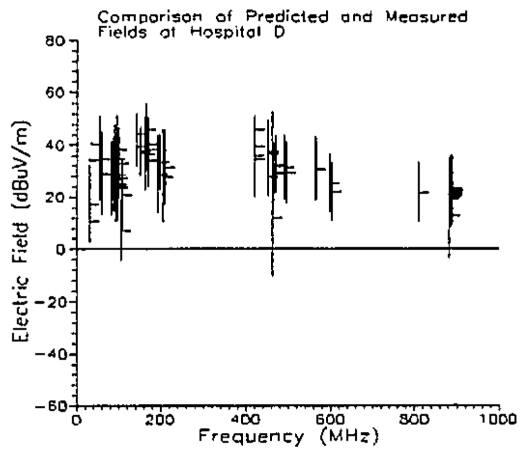

(d) Hospital D

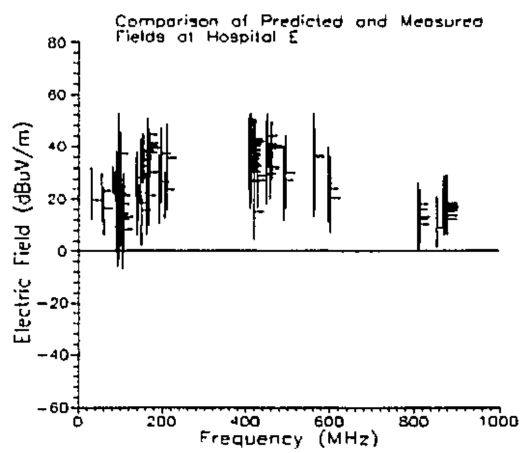

(e) Hospital E

FIGURE 3.3: *Difference between predicted and measured fields (dB).*

DISCUSSION

The prediction method assumed all channels to be active and operating at full power at all times, but several frequency ranges are commuted (not always active). These ranges are: below 50 MHz; between 138-174 MHz; between 400-470 MHz; and between 806-890 MHz. Accordingly, the graphs in figure 3.3 show the largest differences between measured and predicted fields occurred around 150 MHz, 450 MHz, and 850 MHz.

Also, figure 3.3 shows that sometimes the measured field exceeded the predicted field, represented by a value below zero. This occurred primarily in the FM band and might have been caused by additive multipath propagation of the signal.

It was demonstrated in chapter two that both the average and maximum measured field levels were consistently highest in the FM and TV bands (table & figure 2.2). Predicted fields also tended to be highest in these bands, although actual measured field strengths were often greater than estimated. As a result, it is reasonable to conclude that the largest contributions to the EME of hospitals in Montreal will be made by emissions in the FM and TV bands, if the EMI due only to a single channel is of concern. It is unknown whether a similar situation would exist in other cities.

If 'broadband' interference is an issue, as mentioned in chapter two, it should be noted that in the case of the cellular telephone service (806 - 890 MHz), the predicted/measured comparisons (figure 3.3) are seen to be sparse, due to the conditions existing at the time of measurement. If heavy traffic conditions had existed, this band would have been solidly "filled in" on the graphs, thus intensifying a potential broadband EMI effect. It is to be noted also that in one case (Hospital D), the measured fields exceeded those predicted in this band.

It is clear that a prediction method using line-of-sight free-space propagation does not closely estimate the actual fields that propagate through a complex urban environment characterized by buildings and/or natural landforms. Consequently, a field prediction method which more closely estimates actual (measured) field levels will be desired. The resulting method will necessarily be more complex. The next chapter will enumerate the most obvious deficiencies of the LOS method, along with feasible modifications. Finally, the details of a more complex method will be presented, and the performance of both methods will be compared.

Furthermore, the scope of field prediction and measurement will be narrowed to include only FM and television emissions at survey locations <u>outside</u> a hospital.

Chapter 4

FIELD PREDICTIONS USING A HYBRID METHOD

GENERAL

The discrepancies observed, in chapter three, between fields predicted assuming free-space line-of-sight propagation and measured fields, demonstrated the need for a more complex prediction method to obtain better agreement to the measured fields at the hospitals. Such a method should allow a closer characterization of the electromagnetic environment at a hospital.

The LOS prediction method does not account for two obvious additional propagation effects inherent to an urban environment. These are: (1) diffraction caused by human-made and natural obstacles (buildings and hills, respectively); and (2) multipath propagation and scatter from random groupings of intervening structures.

Signal degradation due to diffraction can be compensated for by using geometric (ray) optics analysis, in particular making use of the Uniform Geometric Theory of Diffraction (UGTD) [8]. The intervening structure(s) is modeled in its simplest case as an infinitely conducting half-plane of diffraction, which is among the basic canonical forms to solve. The method is most effective for short transmitter-to-site separation distances (one kilometre), where structures obstructing the propagation path can be easily identified.

When separation distances increase (greater than one kilometre), the urban landscape between the transmitter and the survey location is often densely populated by buildings of quasi-uniform height characterized by the fact that no one building rises significantly above the rest. This condition is known as urban clutter, which can be compensated for by employing known urban clutter coefficients [9].

A hybrid method is proposed which uses a line-of-sight propagation model as its foundation, but attempts to compensate for diffraction and scattering where possible, by utilizing UGTD and urban clutter modeling, respectively. The two compensating components will be described, and predictions generated for exterior sites at the hospitals will be compared to both the measured fields and the LOS predicted fields. Only exterior sites will be considered since they provide the worst-case measure of the electromagnetic environment at a hospital, and bypass the additional complexity of considering signal penetration into buildings which provides the subject for a separate study. Similarly, only frequencies in the FM and television bands will be considered since these signals were observed to be the strongest recorded and so pose a significant risk which may cause medical equipment malfunction in the hospitals (subject to the previously mentioned caveat regarding broad-band effects).

DEVELOPMENT of the HYBRID METHOD

Assessment of the paths to the main known fixed transmitters falls into three categories: (1) true line-of-sight, (2) obstruction due to large, lone or grouped, multistory buildings, or prominent hills, and (3) obstruction due to grouped buildings which cannot be separated from the clutter of the urban landscape. Accordingly, the hybrid method combines three propagation models: (1) a simple line-of-sight (LOS) model, (2) a model based on Kouyoumjian and Pathak's Uniform Geometric Theory of Diffraction (UGTD) [8], and (3) an urban clutter model from Skomal and Smith [9]. Each portion of the hybrid method was applied when appropriate conditions existed.

METHODS

THE UGTD MODEL

A side of a building obstructing the transmitter-to-survey site propagation path can be modeled as a vertical edge of diffraction. The whole building, although of finite dimensions, is collapsed in depth, and modeled as an infinitely conducting half-plane extending away from the edge.

The validity of applying geometric optics, and collapsing the building into a plane, is justified by comparing the wavelength of the propagating signal to the depth of the building. The guideline for applying UGTD is that the structure depth must be ten or more times the signal propagation wavelength. Buildings considered to cause appreciable obstruction were typically fifty metres (or more) deep. The lowest operating frequency in the FM band was 90.3 MHz with a wavelength of 3.3 metres, while in the TV band, a lowest frequency of 55.25 MHz has an associated wavelength of 5.4 metres. This guideline criterion is thus satisfied.

Similarly, hills can be modeled as infinitely conducting half-planes with horizontal diffraction edges parallel to the earth's surface. Topographical information of the terrain between the transmitter and survey location is required to properly identify the location of the edge. Edge location is a matter of judgment and estimation, since some terrain profiles do not clearly indicate a single position where diffraction will occur. In this study, the location of the diffracting edge was assumed to be the position at which lines drawn from both the transmitter and the site intersect the terrain, and are maximally deflected from the straight path, with either line passing through as little terrain as possible. Figure 4.1 shows an example.

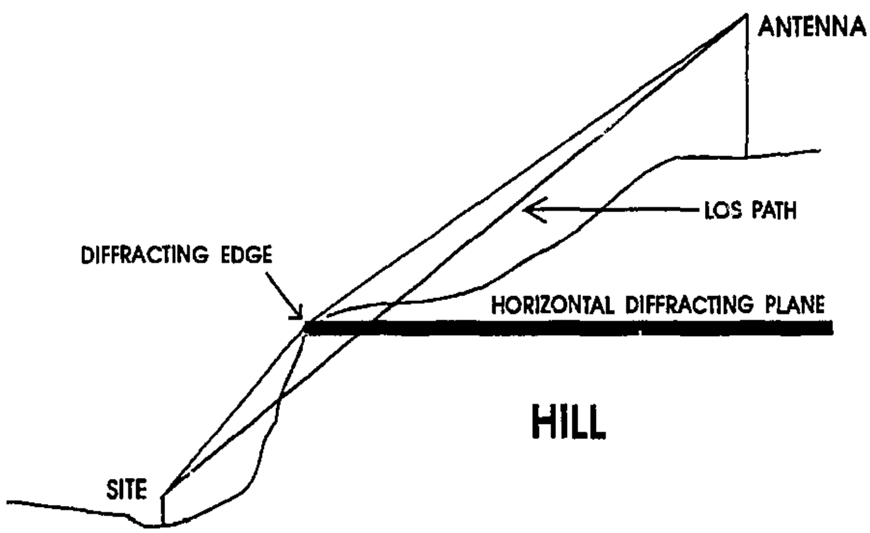

FIGURE 4.1: *Profile of terrain (hill) with diffracting edge and plane identified.*

Topographical information was obtained by consulting publicly available maps from the Bibliothéque Nationale du Québec archives. The maps were produced by Service de l'Habitation et de l'Urbanisme de Montréal in a scale of 1:1000, revised in 1990. The information was manually digitized to obtain computer plotted terrain profiles.

Once the geometry was established, the distances and angles which the transmitter and survey location form with the plane, along with the frequency and the radiated power of the transmitted signal, served as input to a specially developed C++ program to calculate the value of the field at the site.

The Total Field

The total field, E^T, at the field point, or site, is the phasor summation of the direct, reflected, and diffracted fields. The first two field components, E^i and E^r, are contributions due to the geometric optics field [8,10]. The third field component, E^d, is generated by the diffracted field. So,

$$E^T = E^i * u^i + E^r * u^r + E^d \tag{4.1}$$

where u^i and u^r take on a value of one when the field point is illuminated by a direct ray or reflected ray, respectively, and zero otherwise. A diffracted field contribution is always present.

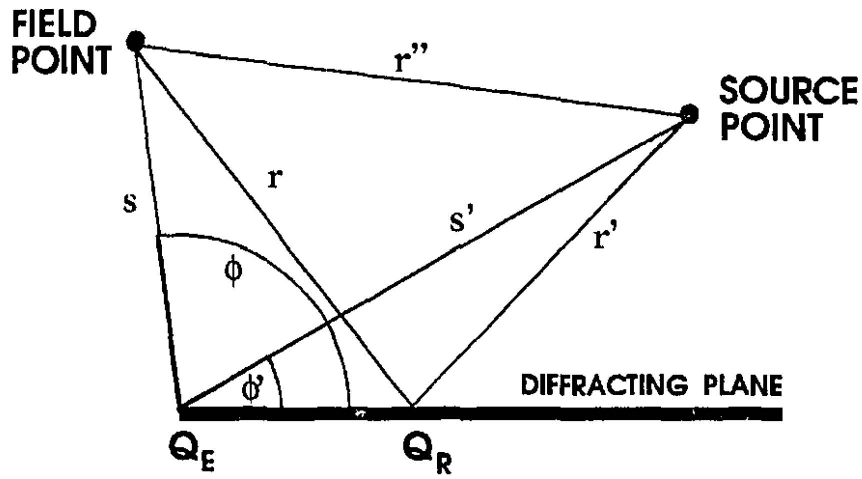

FIGURE 4.2: *Geometry of the source and field points relative to the diffracting plane.*

The UGTD model was employed in situations where the field point was completely hidden by the diffracting plane, and so only a diffracted field contribution existed. However, each of the three components, E^i, E^r, and E^d, is fully developed in equations 4.2-4.10 to illustrate their similar mathematical formulation.

The Geometric Optics (GO) Field

The first two contributions to the total field, E^T, at the field point (survey site) are due to the direct and reflected rays described by geometric optics [10]. Figure 4.2 illustrates the relevant geometry for the GO and diffracted fields.

Allowing the field radiated by the source to be represented as $E^o(0)$, then the field contribution from the incident ray is,

$$\begin{bmatrix} E_{\parallel}^{i}(r'') \\ E_{\perp}^{i}(r'') \end{bmatrix} = \begin{bmatrix} 1 & 0 \\ 0 & 1 \end{bmatrix} \begin{bmatrix} E_{\parallel}^{o}(0) \\ E_{\perp}^{o}(0) \end{bmatrix} \frac{e^{-jkr''}}{r''} \tag{4.2}$$

where r'' is the source to field point distance, and $E_{\parallel}$ and $E_{\perp}$ indicate waves of parallel and perpendicular polarization. The half-plane reflects the incident ray at a point, Q_R, where θ^r (angle of reflection) = θ^i (angle of incidence), adding a field of

$$\begin{bmatrix} E_{\parallel}^{r}(r) \\ E_{\perp}^{r}(r) \end{bmatrix} = \begin{bmatrix} 1 & 0 \\ 0 & -1 \end{bmatrix} \begin{bmatrix} E_{\parallel}^{i}(Q_R) \\ E_{\perp}^{i}(Q_R) \end{bmatrix} \frac{e^{-jkr}}{r} \tag{4.3}$$

where r is the distance from Q_R to the field point.

Also,

$$\begin{bmatrix} E_{\parallel}^{i}(Q_R) \\ E_{\perp}^{i}(Q_R) \end{bmatrix} = \begin{bmatrix} 1 & 0 \\ 0 & 1 \end{bmatrix} \begin{bmatrix} E_{\parallel}^{o}(0) \\ E_{\perp}^{o}(0) \end{bmatrix} \frac{e^{-jkr'}}{r'} \tag{4.4}$$

where r' is the distance from the source to Q_R.

The Diffracted Field

The third component of the total field at the field point is due to diffraction from an infinitely conducting semi-infinite half-plane assuming a planar incident wave, described by

$$\begin{bmatrix} E_{\parallel}^{d}(s) \\ E_{\perp}^{d}(s) \end{bmatrix} = \begin{bmatrix} -D_s & 0 \\ 0 & -D_h \end{bmatrix} \begin{bmatrix} E_{\parallel}^{i}(Q_E) \\ E_{\perp}^{i}(Q_E) \end{bmatrix} \frac{e^{-jks}}{\sqrt{s}} \tag{4.5}$$

where s is the distance from Q_E, the edge diffraction point, to the field point. The field at Q_E due to the source is

$$\begin{bmatrix} E_{\parallel}^{i}(Q_E) \\ E_{\perp}^{i}(Q_E) \end{bmatrix} = \begin{bmatrix} 1 & 0 \\ 0 & 1 \end{bmatrix} \begin{bmatrix} E_{\parallel}^{o}(0) \\ E_{\perp}^{o}(0) \end{bmatrix} \frac{e^{-jks'}}{s'} \tag{4.6}$$

where s' is the distance from the source to Q_E.

The diffraction coefficients, D_s and D_h, indicate the acoustically *soft* and *hard*, or Dirichlet and Neumann boundary condition cases, and correspond to incident waves which are *parallel* and *perpendicular* polarized, respectively. The equations for determining these coefficients are reproduced from Kouyoumjian and Pathak [8] below.

$$\begin{aligned} D_{s,h}(\varphi,\varphi';\beta_o) = \frac{-e^{-j\pi/4}}{2n\sqrt{2\pi k}\sin\beta_o} \times \Bigg[& \cot\left(\frac{\pi+(\varphi-\varphi')}{2n}\right) F[kLa^{+}(\varphi-\varphi')] \\ & + \cot\left(\frac{\pi-(\varphi-\varphi')}{2n}\right) F[kLa^{-}(\varphi-\varphi')] \\ & \mp \left\{ \cot\left(\frac{\pi+(\varphi+\varphi')}{2n}\right) F[kLa^{+}(\varphi+\varphi')] \right. \\ & \left. + \cot\left(\frac{\pi-(\varphi+\varphi')}{2n}\right) F[kLa^{-}(\varphi+\varphi')] \right\} \Bigg] \end{aligned} \tag{4.7}$$

where

$$F(X) = 2j\sqrt{X}\, e^{jX} \int_{\sqrt{X}}^{\infty} e^{-jt^2}\, dt \tag{4.8}$$

The positive square root of X is taken.

$$a^{\pm}(\beta_0) = 2\cos^2\left(\frac{2n\pi N^{\pm} - \beta}{2}\right) \tag{4.9}$$

where $N^{\pm}$ are integers from [7] that satisfy

$$2\pi n N^{+} - \beta = \pi \quad \text{and} \quad 2\pi n N^{-} - \beta = -\pi \quad \text{with} \quad \beta = \varphi \pm \varphi'. \tag{4.10}$$

$F(X)$ is a variation of the Fresnel integral and is evaluated by numerical integration. The function L contained in the Fresnel integral is a distance parameter given by $L = s \sin^2 \beta_0$ for plane wave incidence, where s was defined in figure 4.2. β_0 is the angle of elevation of the incident signal in a plane parallel to, and passing through the edge of diffraction. For simplicity, normal incidence to the plane of diffraction is assumed. Therefore, with $\beta_0 =$ 90 degrees, $L = s$. φ and φ' are the angles formed, in the plane perpendicular to the edge, by the field and source points, respectively, relative to the semi-infinite half-plane. The wave number is represented as k. The equations are presented without a fully detailed explanation of the variables involved or the finer points of UGTD solution. For the complete development, the reader is referred to the original paper by Kouyoumjian and Pathak [8]. Note that two results are generated, corresponding to waves of parallel and perpendicular polarization.

Since no information regarding the polarization of the radiated signals is available, the larger (worst case) calculated result is retained.

The Urban Clutter Model

When prominent single, or grouped, interfering structures in the propagation path cannot be distinguished from the clutter of the urban landscape, the field at the survey site, E, is obtained from [9] as

$$E = E_{LOS} - A_{mu} - K_{mr} - H_{tc} - H_{rc} \text{ in dB,} \qquad \textbf{(4.11)}$$

where E_{LOS} is the line of sight prediction; A_{mu} is the basic median attenuation for a quasi-smooth urban area relative to free space; K_{mr} is the suburban correction factor; H_{tc} is the transmitter height gain factor; and H_{rc} is the receiver height gain factor. All factors are obtained using families of graphs presented in [9].

Results and Analysis

Fields were predicted using the LOS and hybrid methods at five exterior sites, in both the FM radio and television bands. Recall that only exterior sites were considered since fields at these sites represented the worst case environment the hospital might experience due to external sources.

A preliminary comparison of fields predicted by both methods to the measurements showed consistent agreement between results in the FM band, but erratic agreement in the TV band. However, this is reasonable since TV signals are composed of a broadband amplitude modulated video signal, and a narrowband frequency modulated audio signal. The temporal variation of the video signal implies that measurements made of this signal can only, at best, indicate an approximate field strength. The FM audio signal, though, should behave in essentially the same way as the signals in the FM radio band. For this reason, the following analysis will restrict itself to the fields predicted and measured in the FM band along with the audio signals in the TV band. These signals will be denoted as the 'FM and TV (audio) band'. It should also be noted that signal compensation for the radiation pattern of the transmitting antenna has been omitted to simplify the analysis.

Table 4.1 shows average FM and TV (audio) field levels and sample standard deviations measured at each site (right), and compares measurements with levels predicted by the LOS method (centre) and the hybrid method (left). Ranks of the averages are shown in brackets. LOS predictions tended to be correlated with measured fields (Spearman Rank Correlation coefficient [9,11], Rs=0.8); hybrid predictions also tended to be correlated (Rs=0.7). However, neither correlation was significantly non-zero.

The same data is presented in a graphical format in figure 4.3, which more readily illustrates the improved performance of the hybrid method. The centered symbols show the average over 18 frequencies at each site, while the error bars indicate the standard deviations from this mean. Site B_1 showed the best performance of the hybrid method, where the average corresponds closely to that of the measured fields. By contrast, the hybrid predictions were not significantly better than the LOS predictions in estimating the actual fields at Site C_1 indicating the relative limitations of the hybrid method. This was due to the location of this site where "tangential" shadowing conditions existed, in the sense that the propagation path was below the tangent to the shadowing surface which was covered by trees.

The LOS predictive method was clearly dominant at Site C_2 which was on the roof-top of a tall hospital building in true line-of-sight from the transmitters, thus providing virtual "antenna range" conditions. Field levels were predicted to within about 10 dB.

A comparison of the predicted and measured fields in the FM band alone is presented in table 4.2 and figure 4.4. Such a comparison illustrates the improved agreement between the predicted and measured fields, for either prediction method, when the audio portion of the television signals is omitted. This apparent anomaly will be addressed in the **DISCUSSION** section.

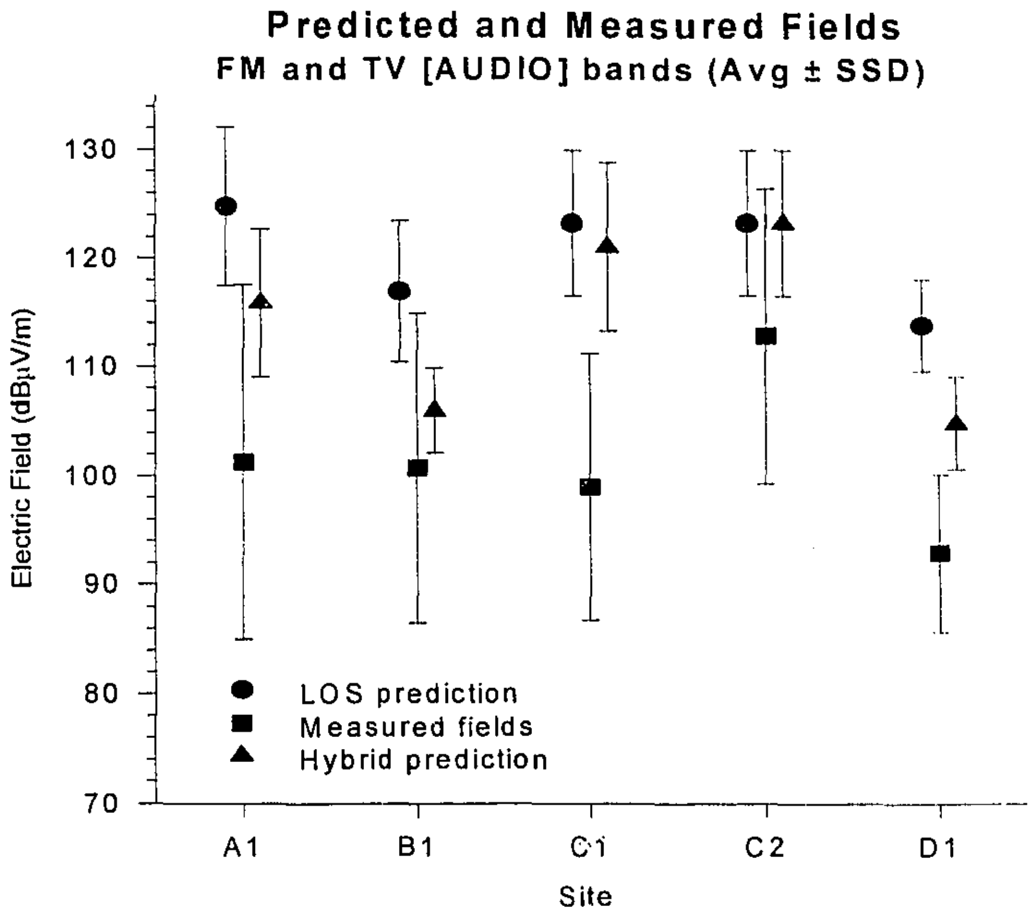

FIGURE 4.3: *Comparison of predicted and measured fields in the FM and TV (audio) bands.*

Site	Hybrid Method Average ± SSD (Rank)	LOS Method Average ± SSD (Rank)	Measured Average ± SSD (Rank)
A_1	115.88 ± 6.84 (3)	124.79 ± 7.32 (1)	101.30 ± 16.28 (2)
B_1	106.01± 3.88 (4)	116.96 ± 6.54 (4)	100.76 ± 14.19 (3)
C_1	121.10 ± 7.76 (2)	123.29 ± 6.69 (3)	99.02 ± 12.24 (4)
C_2	123.35 ± 6.70 (1)	123.35 ± 6.70 (2)	112.93 ± 13.56 (1)
D_1	104.94 ± 4.25 (5)	113.94 ± 4.25 (5)	92.98 ± 7.26 (5)

TABLE 4.1: *Comparison of predicted and measured fields in the FM and TV (audio) bands in dBµV m.*

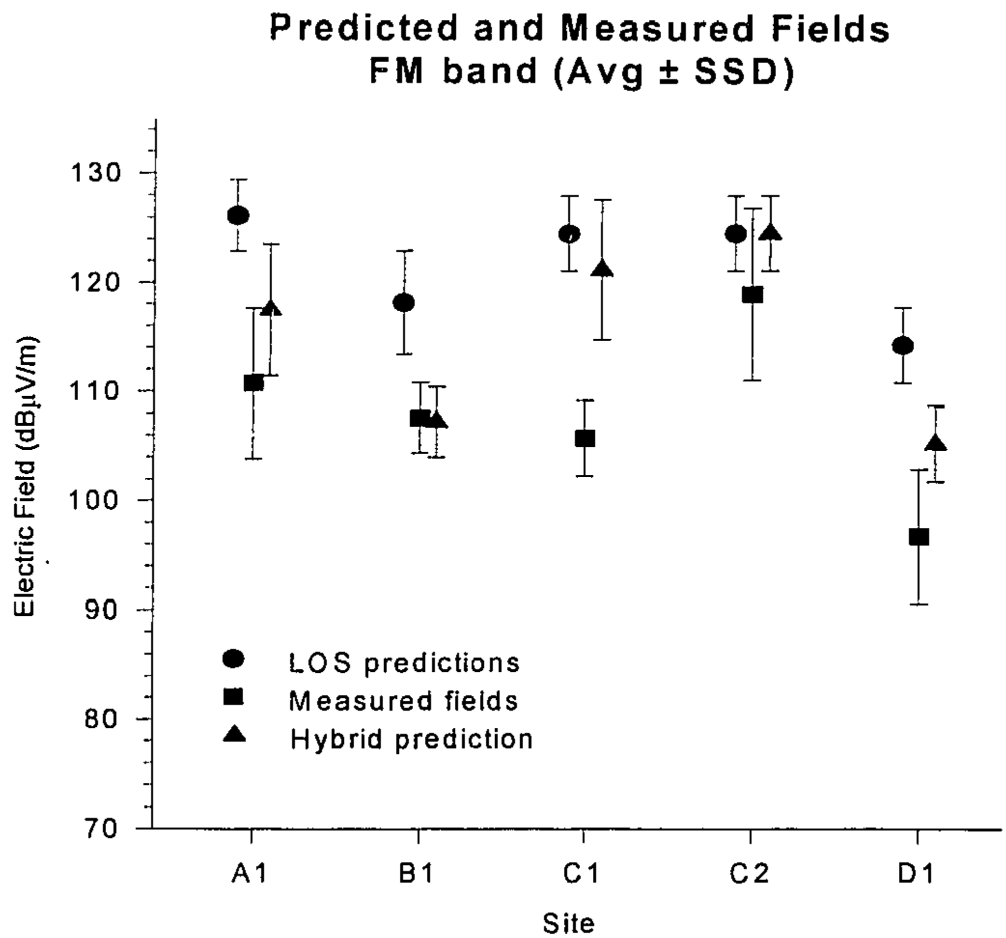

FIGURE 4.4: *Comparison of predicted and measured fields in the FM band.*

Site	Hybrid Method Average ± SSD (Rank)	LOS Method Average ± SSD (Rank)	Measured Average ± SSD (Rank)
A_1	117.48 ± 6.07 (3)	126.16 ± 3.24 (1)	110.72 ± 6.89 (2)
B_1	107.21 ± 3.19 (4)	118.19 ± 4.76 (4)	107.69 ± 3.18 (3)
C_1	121.16 ± 6.43 (2)	124.51 ± 3.24 (3)	105.72 ± 3.43 (4)
C_2	124.58 ± 3.42 (1)	124.58 ± 3.42 (2)	118.96 ± 7.92 (1)
D_1	105.30 ± 3.47 (5)	114.30 ± 3.47 (5)	96.77 ± 6.16 (5)

TABLE 4.2: *Comparison of predicted and measured FM field levels in dBμV/m.*

The data contained in tables 4.1 & 4.2 and figures 4.3 & 4.4 can be presented in a different format which illustrates more clearly the performance of each predictive method over the different frequency bands. In tables 4.3 & 4.4, and figures 4.5 & 4.6, the measured fields have been subtracted from the fields predicted by each method in the FM and TV (audio) bands and FM band respectively, showing only the difference between the predictions and measurements.

Specifically, table 4.3 compares the average differences in the FM and TV (audio) bands between the predicted and measured fields for the LOS method (right column) and hybrid method (centre). Sample standard deviations (SSD) over the averages (N=18) are also indicated. A graphical representation of the information contained in table 4.3 appears in figure 4.5. The dashed horizontal line through zero indicates a 'perfect prediction' where there is zero difference between the predicted and measured fields.

Similarly, table 4.4 shows the average differences and sample standard deviations in the FM band only. Figure 4.6 presents this information graphically. As indicated previously, the rationale for showing the results for the FM band both with and without the television audio signal was to illustrate the improvement in agreement between the predicted and measured fields when the TV audio signal is excluded. This anomaly is discussed later.

Site C_2 was the only location where all transmitter antennas could be seen, and no correction to the LOS model was necessary. Three of five sites employed

UGTD results for the predicted field. At site A_1, terrain that obstructed a clear view of several transmitters was modeled as a horizontal half-plane (UGTD-H). At site B_1, a majority of the FM transmitting antennas was obscured from view by a single multistory structure, so that a vertical half-plane model was employed (UGTD-V). Site C_1 combined both vertical and horizontal half plane modeling due to obstruction caused by the hospital itself and intermediate terrain, respectively, as well as LOS predictions at most frequencies. At site D_1, an urban scatter model was appropriate. The clutter loss factor was in the order of nine dB. The improved agreement of the hybrid method predictions to the measured fields was evident at sites A_1, C_1, and D_1, but most notably at site B_1. Table 4.4 and figure 4.6 show the differences between the predicted and measured fields in the FM band only.

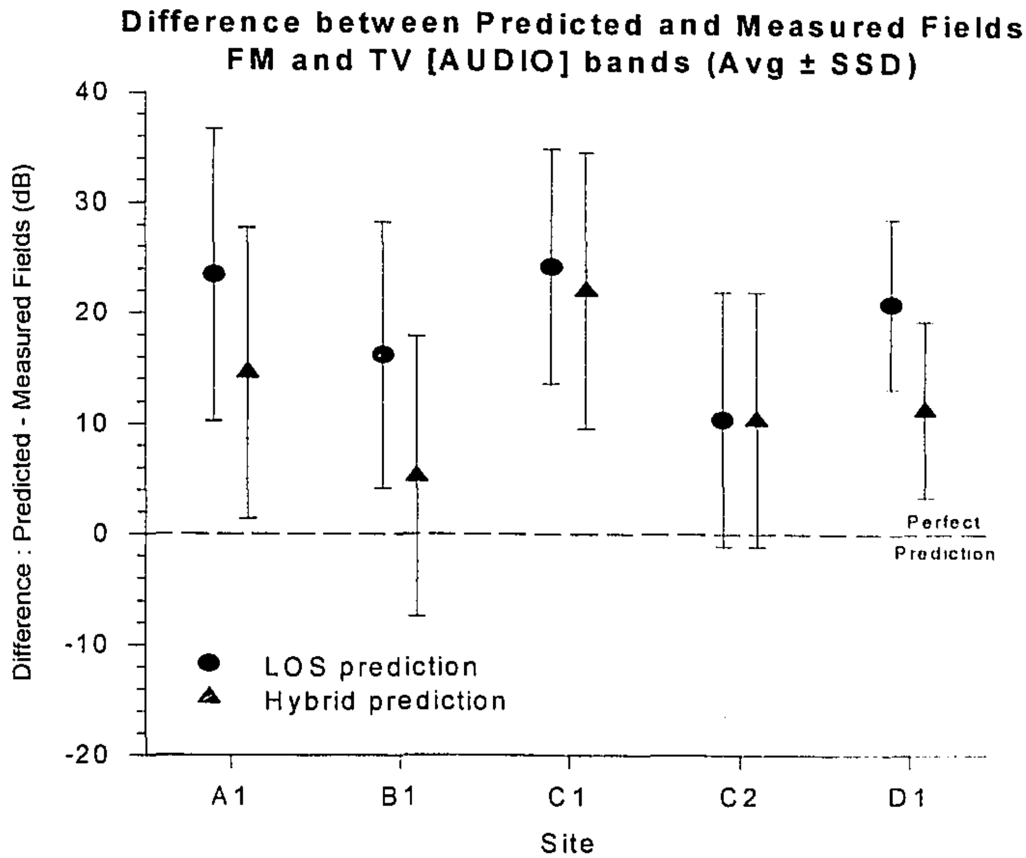

FIGURE 4.5: *Difference between predicted and measured fields in the FM and TV (audio) bands.*

Site	Hybrid-Measured		LOS-Measured
	Model	Average ± SSD	Average ± SSD
A_1	UGTD-H	14.58 ± 13.15	23.48 ± 13.21
B_1	UGTD-V	5.24 ± 12.66	16.20 ± 12.07
C_1	LOS UGTD-V/H	22.08 ± 12.51	24.26 ± 10.66
C_2	LOS	10.43 ± 11.55	10.43 ± 11.55
D_1	Clutter	11.33 ± 7.98	20.96 ± 7.71
All		12.73 ± 6.21	19.07 ± 5.76

TABLE 4.3: *Comparison of E-field prediction errors for different methods averaged over the FM and TV (audio) bands (dB).*

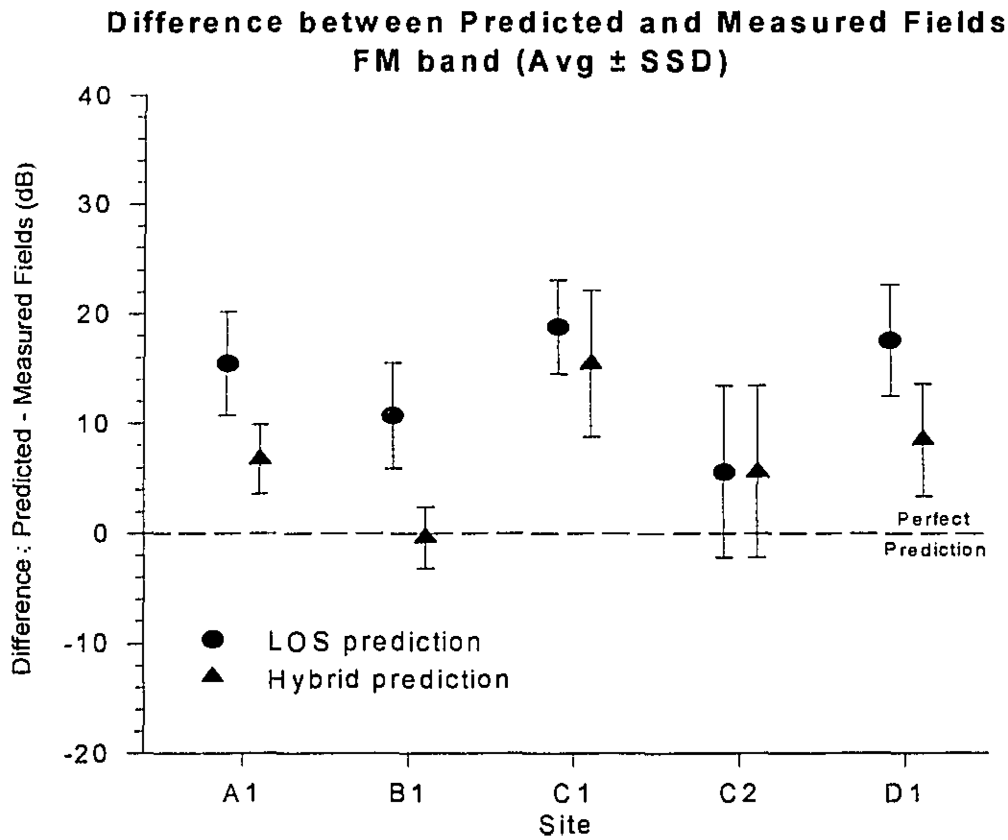

FIGURE 4.6: *Difference between predicted and measured fields in the FM band.*

Site	Hybrid-Measured Model	Hybrid-Measured Average ± SSD	LOS-Measured Average ± SSD
A_1	UGTD-H	6.76 ± 3.12	15.44 ± 4.75
B_1	UGTD-V	-0.39 ± 2.83	10.60 ± 4.80
C_1	LOS UGTD-V/H	15.44 ± 6.69	18.79 ± 4.28
C_2	LOS	5.62 ± 7.82	5.62 ± 7.82
D_1	Clutter	8.52 ± 5.10	17.52 ± 5.10
All		7.19 ± 7.36	13.59 ± 7.22

TABLE 4.4: *Comparison of E-field prediction errors for different methods averaged over the FM band (dB).*

DISCUSSION

Figures 4.3-4.6 demonstrate the improved agreement between the predicted and measured fields when the hybrid prediction method was used. This is particularly noticeable at Sites A_1, B_1, and D_1, with marginal improvement at Site C_1. The suitability of the UGTD component of the hybrid method was acutely apparent at Site B_1, where all predictions were made utilizing only this component. The urban clutter component demonstrated its merits in application at Site D_1, while Site A_1 showed how the combination of LOS and UGTD components can improve the accuracy of the fields predicted.

The signal paths from the transmitters on Mount Royal to Site C_1 were such that "tangential" shadowing was dominant. In addition, there was multipath reflection both from buildings and the mountain itself. None of the three propagation models which comprise the hybrid method sufficiently described the propagation conditions at this site, resulting in poor performance. However, this is a good indication of how well the hybrid method can be expected to perform in 'difficult' situations. On average, the hybrid method generated predictions to within roughly 13 dB of the measurements in the FM and TV (audio) bands.

The LOS method demonstrated its suitability at Site C_2 which was in full line-of-sight view of the transmitters, by predicting fields to within about 10 dB of the measured fields. The LOS predictions, averaged over the five sites, came to within about 20 dB of the measured fields.

Figures 4.4 & 4.6 and corresponding tables 4.3 & 4.4 have been included to illustrate the improved performance of either method when only the FM band was considered. Table 4.4 indicates that fields in the FM band could be predicted to within about 14 dB using the LOS method, and to within about 7 dB by the hybrid method. It is important to realize that the FM band spans only 88-108 MHz, which is a small range compared to the television band, which begins at 55.25 MHz and has frequency assignments until 601.75 MHz. This suggests that a further examination of the propagation models used for the broad range of frequencies assigned for television services (a 10:1 ratio) is required.

Therefore, the next section will make use of a modified propagation model which is both separation distance and frequency dependent. Results will be generated for the same five exterior survey locations using this modified model, both alone and as incorporated into the hybrid method. Both methods will be evaluated by a comparison to the measured and previously predicted fields.

Chapter 5

FIELD PREDICTIONS USING A MODIFIED LOS COMPONENT

GENERAL

Comparison of fields predicted by both the LOS and hybrid methods to the measured fields demonstrated that the accuracy of the hybrid method was limited primarily by the performance of the LOS component. The current line-of-sight model completely describes the propagation of the radiated signal in free space, but disregards the effects of the transmitting and receiving antennae. The transmitting antenna need not be considered since its antenna characteristics are embedded into the value for the effective isotropic radiated power. However, the line-of-sight model can be somewhat refined by considering the effects of the receiving antenna on the transmission system, as proposed by Skomal and Smith [9]. A more involved, yet generally applicable, formulation is presented in Stutzman and Thiele [10, p.57-61] which accounts for contributions from both transmitting and receiving antennae used in communication links.

In this chapter, a 'modified' line-of-sight free-space propagation component (*LOS B*) will be employed, and its performance evaluated over the FM radio and television bands, for the measurements made outside the hospitals. This 'modified' LOS model will also be substituted into the hybrid method, replacing the earlier LOS component. The performance of the corresponding modified hybrid method, labeled *Hybrid B*, will also be evaluated.

METHODS

The literature [9,10] suggests a method of accounting for the properties of the transmitting and receiving antennae in a line-of-sight communication, based on antennae gain and operating frequency. Since transmitter gain and radiated power information is combined in effective radiated power data, only the effects of the receiving antenna remain for consideration. Thus, assuming an isotropic receiving antenna of unity gain, the received power, P_R, as proposed in [9,10], is given by

$$P_R \doteq P_T \left(\frac{\lambda}{4\pi r} \right)^2 \qquad \textbf{(5.1)}$$

where P_T is the effective isotropic radiated power of the transmitter [9,10]. This equation is often used in its logarithmic form, given by

$$P_R(dBW) = P_T(EIRP\ in\ dBW) - 20\log(f_M) - 20\log(d_K) - 32.44 \qquad \textbf{(5.2)}$$

where P_T is the effective isotropic radiated power , f_M is the frequency in megahertz, and d_K is the LOS transmitter-to-survey site distance in kilometres [9,10]. The power is readily converted into the expected electric field, E_R in dBμV/m, at the site.

The figures and tables in the following section will include, as in chapter three, the results for sites outside of four hospitals only, although measurements were made at five. Recall that in the case of Hospital C, fields at two sites, C_1 and C_2, were measured. In the case of Hospital E, no results are presented since in the course of analysis it was found that the measurements for the <u>outdoor</u> site were invalid, due to equipment failure. This equipment failure, however, was corrected for the <u>indoor</u>

measurements at Hospital E. The experience of measurement failure further supports the need for developing predictive methods and using them, when appropriate, in conjunction with measurements.

RESULTS and ANALYSIS

Results are presented for FM and TV (audio) frequencies, and also for FM and TV (audio and video) frequencies for two reasons: (1) the poor performance, in the TV band, of the hybrid A method presented in the previous section may be attributed to the large range of frequencies which the television signals span, and (2) good performance was noted for both bands when transmission frequency was taken into consideration.

As in chapter four, the measured fields were subtracted from the fields predicted by each method ($E_{predicted}$ - $E_{measured}$) at each of the five outdoor locations. Average differences and sample standard deviations were calculated to assess the performance of each method.

Figure 5.1 and table 5.1 show averages and standard deviations for the FM and TV (audio) band. Similar results for the FM and TV (audio & video) band are tabled and graphed in table 5.2 and figure 5.2. Note that the horizontal line through zero indicates a 'perfect prediction' where there is zero difference between the predicted and measured fields.

The following nomenclature is used in these tables and figures:

(i) LOS A corresponds to the frequency *independent* LOS prediction method ;

(ii) LOS B implies an LOS method which depends on *both* frequency and separation distance;

(iii) Hybrid A is the method presented in the previous section, using LOS A; and,

(iv) Hybrid B is a method incorporating the *frequency dependent* LOS model (LOS B), a UGTD model, and an urban clutter model.

Tables 5.1 & 5.2 and figures 5.1 & 5.2 present averaged values which do not fully describe the relationships between the predicted and measured fields. Information concerning the performance of each prediction method on a frequency-by-frequency basis is lost. That is not to say that the previous averaged values do not effectively describe the performance of each method, but rather, that further information about how each method performs can be gleaned through scatter plots comparing the predicted fields to the measured fields for each frequency under consideration. Figure 5.3 shows the scatter plots for site A_1 over the FM and television (audio) band, which contains information used in table 5.1 and figure 5.1. Each graph shows the fields predicted by one of the four methods compared to the actual measured fields. Ideally, a one-to-one relationship should exist. This relationship is indicated on each graph by a reference line of slope one. Note that subtracting the measured field from the predicted field, as was done to obtain the results in table 5.1, is equivalent, graphically, to measuring the vertical separation between the plotted points and the unity slope line. The graphs for site A_1 are presented as an example. Similar graphs were obtained for each site.

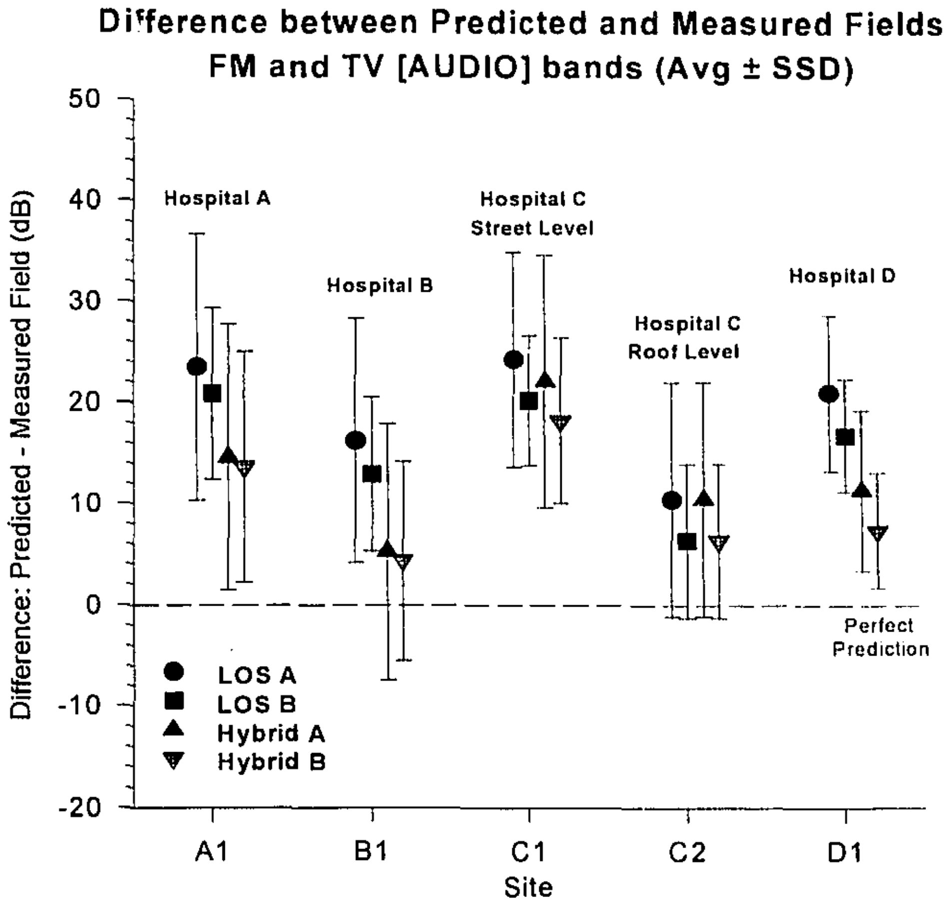

FIGURE 5.1: *Predicted minus measured fields for FM and TV (audio) bands comparing all four prediction methods.*

Site	LOS A - Meas Average ± SSD	LOS B - Meas Average ± SSD	Hybrid A - Meas Average ± SSD	Hybrid B - Meas Average ± SSD
A_1	23.48 ± 13.21	20.86 ± 8.49	14.58 ± 13.15	13.59 ± 11.42
B_1	16.20 ± 12.07	12.87 ± 7.58	5.24 ± 12.66	4.33 ± 9.83
C_1	24.26 ± 10.66	20.20 ± 6.41	22.08 ± 12.51	18.24 ± 8.17
C_2	10.43 ± 11.55	6.34 ± 7.59	10.43 ± 11.55	6.34 ± 7.59
D_1	20.96 ± 7.71	16.78 ± 5.57	11.33 ± 7.98	7.37 ± 5.70
All	19.07 ± 12.11	15.41 ± 8.86	12.86 ± 12.70	10.06 ± 9.98

TABLE 5.1: *Predicted minus measured fields for FM and TV (audio) bands comparing all four prediction methods (dB).*

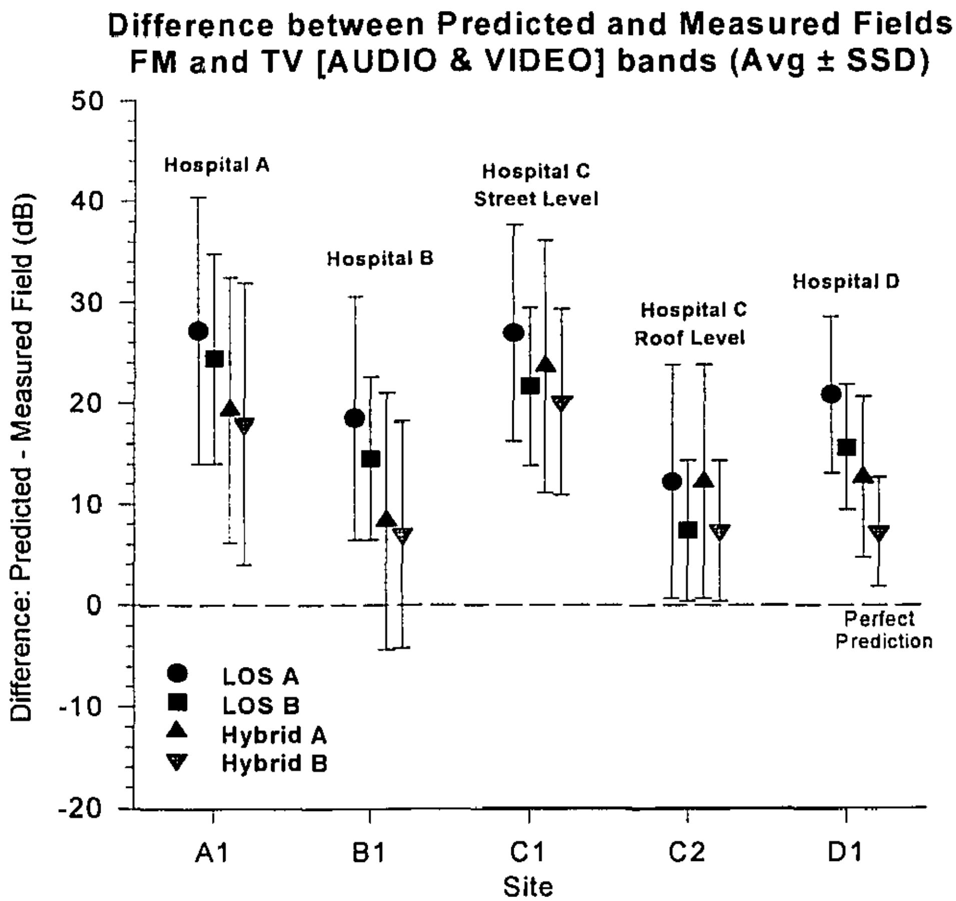

FIGURE 5.2: *Predicted minus measured fields for FM and TV (audio & video) bands comparing all four prediction methods.*

Site	LOS A - Meas Average ± SSD	LOS B - Meas Average ± SSD	Hybrid A - Meas Average ± SSD	Hybrid B - Meas Average ± SSD
A_1	27.22 ± 16.23	24.44 ± 10.40	19.33 ± 15.68	17.96 ± 13.97
B_1	18.52 ± 13.82	14.54 ± 8.07	8.34 ± 14.68	7.02 ± 11.17
C_1	26.92 ± 12.14	21.63 ± 7.79	23.62 ± 14.25	20.12 ± 9.19
C_2	12.21 ± 11.56	7.39 ± 6.97	12.21 ± 11.56	7.39 ± 6.97
D_1	20.83 ± 9.22	15.64 ± 6.18	12.66 ± 8.35	7.26 ± 5.41
All	21.60 ± 13.58	16.72 ± 9.86	15.66 ± 14.17	11.95 ± 11.30

TABLE 5.2: *Predicted minus measured fields for FM and TV (audio & video) bands comparing all four prediction methods (dB).*

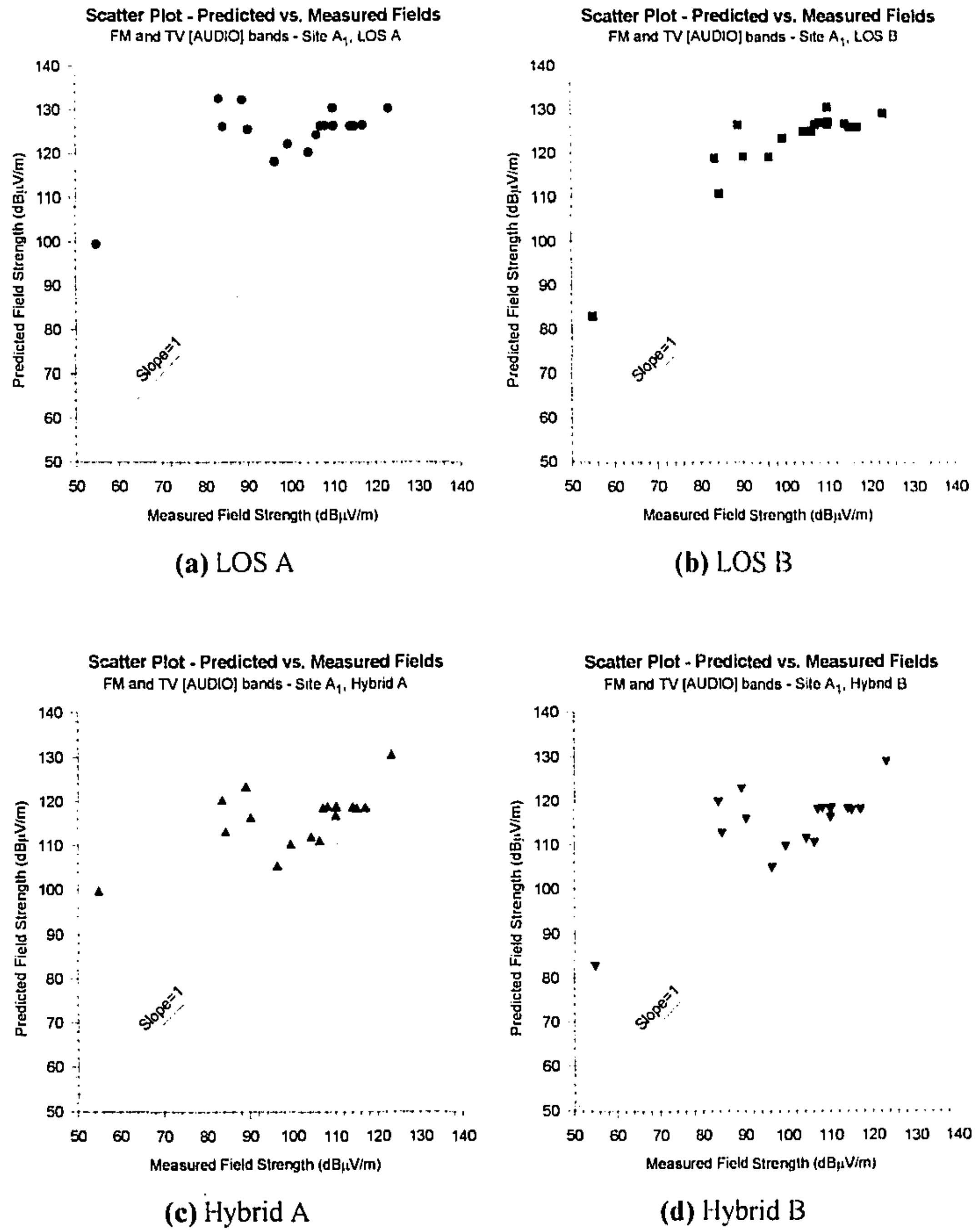

FIGURE 5.3: *Scatter plots of predicted and measured fields for site A_1 in the FM & TV (audio) bands:* ***(a)*** *LOS A,* ***(b)*** *LOS B,* ***(c)*** *Hybrid A,* ***(d)*** *Hybrid B.*

The graphs of figure 5.3 support the findings presented in table 5.1 and figure 5.1 in that the scattered points align more closely to the line of unity slope using the LOS B method, than using the LOS A method.

Figure 5.3 shows a significant outlying point on the left-hand side near 55 dBμV/m on the horizontal axis. It consistently deviated from the unity slope line for all five sites.

DISCUSSION

In figure 5.3, a comparison of the LOS methods to the hybrid methods demonstrated the effectiveness of the hybrid methods in bringing the predicted values closer to the unity slope line. It should be noted that the predictions made using the hybrid methods employed the UGTD component almost exclusively due to the location of the survey site relative to the transmitters.

The outlying data point near 55 dBμV/m on the horizontal axis is attributable to a television station between 500 - 600 MHz, whose distance from the survey sites was supplied by Industry Canada, but where precise geographic location was not documented and thus the intervening terrain could not be exactly characterized. However, general location information indicates that the particular transmitter was obstructed from all five sites by a significant intervening natural landform (Mount Royal and urban clutter), thus explaining the resultant inaccuracy of any of the four methods. Uncertainty about the location of this transmitter made it impossible to attempt compensation using the UGTD model. The data point was retained as an example of a situational difficulty which may be encountered in practice.

Furthermore, the cluster of four points forming a parallelogram in the 80 - 90 dBμV/m range on the Measured Field Strength axis were also relatively distant from the line of unity slope, and were also produced by television transmitters. This behaviour was most marked at site A_1, presented in figure 5.3. As mentioned previously, similar scatter plots were also produced for sites B_1, C_1, C_2, and D_1, and these indicated a similar general tendency which may have been caused by complexities in the propagation paths that were not accounted for.

Figures 5.1, 5.2 & 5.3 indicate that the frequency dependent LOS prediction method (LOS B) generated results nearer to the measured fields than did LOS A. Estimates of expected fields in the FM and audio television bands could be obtained to within about 20 dB using LOS A, and to about 15 dB using LOS B. Similarly, due to the use of LOS B in the Hybrid B method, it is not surprising that Hybrid B returned predictions closer to the measured fields than did Hybrid A. Hybrid A predicted fields to within 13 dB, and Hybrid B to within 10 dB. Both hybrid methods generated predictions closer to the measured fields than did the LOS methods, as demonstrated in figure 5.3, however at the expense of considerably greater time and effort.

The evolution of the prediction methodology also resulted in simple nomographs (Appendix A) which were produced as by-products of the work. These are graphical tools which can be used for rapidly estimating the EME at a site. These charts, based on the LOS A and LOS B methods, require knowledge of the transmitter effective isotropic radiated power, the transmitter-to-survey site distance, and in the case of LOS B, the transmission frequency. Using these charts, approximate field strengths at a survey site can be rapidly predicted, within the limits outlined above. The charts can also be used to determine equivalencies (power level, distance, resultant field) between fixed and mobile radiators. However, in situations requiring evaluation of UGTD scattering, numerical calculation continues to be needed.

SUMMARY OF PART I

As a step to achieving the long term objective of a harmonious co-existence between critical-care medical equipment in a hospital and modern radiating devices, the relative hostility of the electromagnetic environment caused by external sources at five Montreal area hospitals has been examined by measurement and prediction. Predictions calculated using a simple, free-space, line-of-sight method, have been compared to the measured fields at the five hospitals, representing an amalgamation of the results by Boisvert (three hospitals), and the current results (two hospitals).

Although the initial comparison involved all documented, fixed sources, it became evident that frequencies in the FM and television bands were the strongest recorded, and so posed a significant risk which may cause medical equipment malfunction in the hospitals (subject to the previously mentioned caveat regarding broadband effects).

The previous Boisvert [7] estimates used a simple free-space LOS prediction method which has been extended by considering more realistic propagation conditions. The effectiveness of these improvements has been examined at locations outside the hospitals, thus excluding the additional complexity of attenuation due to signal penetration into the buildings.

Consequently, four computational methods for predicting the EM fields outside hospitals due to neighbouring very high power FM radio and TV transmitters have been examined, with the goal of obtaining simple, meaningful methods of sufficient accuracy to reduce the need for extensive, large-scale measurements.

The four prediction methods were developed from four propagation models which best described the propagation conditions observed at the five hospitals in Montreal. The relation between the models and methods is illustrated in figure 5.4.

A comparison of the fields predicted by each method to the measured fields indicated that a frequency dependent line-of-sight method (LOS B) generated predictions closer to the measured fields than a line-of-sight method with no frequency dependence (LOS A). Similarly, the Hybrid B method performed better than the Hybrid A method. Due to the more realistic propagation modeling used in the hybrid methods, it is not surprising that they showed improved performance in

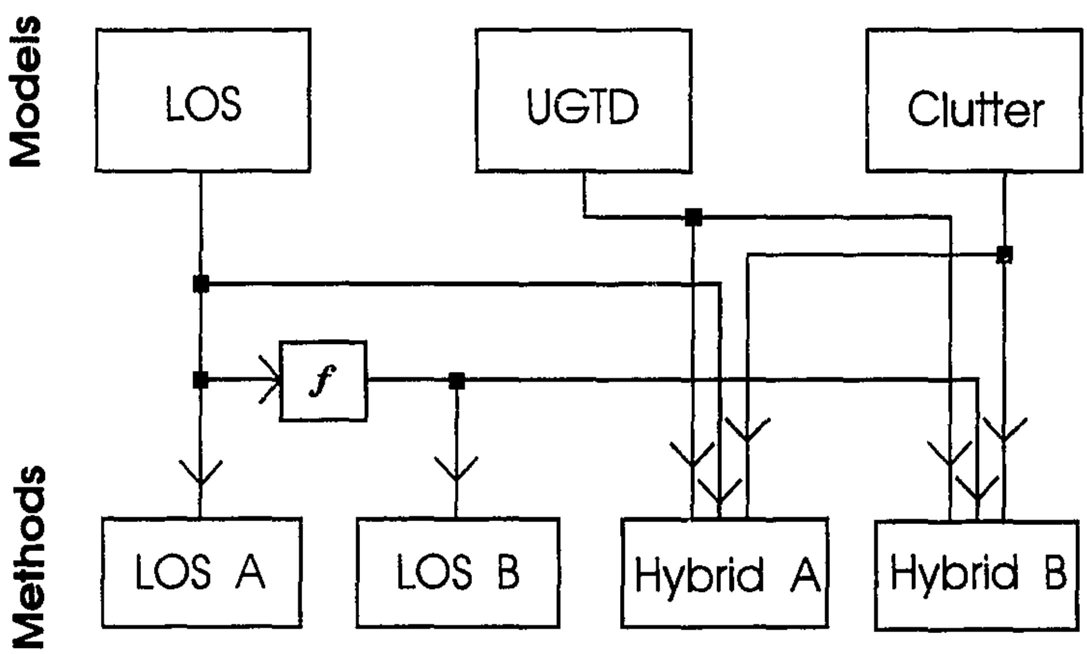

FIGURE 5.4: *Four prediction methods developed from a basis of the propagation models ('f' indicates frequency dependence).*

comparison to the line-of-sight methods. This was achieved, though, at the cost of increased complexity. Overall, the Hybrid B method generated predictions closest to the measured fields (to within about 10 dB on average). It is significant, however, that in most cases, the predicted fields were higher than the measured fields. Also, recall that in attempting to identify EMC hazards at hospitals, the same degree of accuracy is not required as in (point-to-point or cellular) telecommunication systems.

The advantage of using either line-of-sight method is that they <u>easily</u> suggest worst-case susceptibility requirements for the medical equipment in a hospital. Thus, if the equipment operates normally in field levels predicted by either LOS method, it should not malfunction anywhere inside the hospital. The levels at which susceptibility requirements should be set is the topic of much current discussion, and is open to debate.

Until this point in the thesis, only the effects of external sources on the outside and inside electromagnetic environment of a hospital have been considered. Of comparable concern are the effects of sources located inside the hospital, particularly in light of the increasingly widespread use of wireless communicators. The following chapter will analyze measurements of radio wave propagation, made in a modern building that is similar to a hospital, due to radiating sources inside the building site. Specifically, signal propagation will be examined for configurations in which the transmitter and receiver are located on the same floor, and in which they are separated by one to nine floors.

The relationship between the inside fields due to the external electromagnetic environment will not be addressed, other than to say that the internal EME was at least 3 dB lower, in the FM and TV bands, than the external EME for directly exposed hospital buildings. The topic of attenuation of signals penetrating into a building is a major problem for study in its own right.

PART II: The EME due to Internal Sources

Chapter 6

INDOOR PROPAGATION AT 433, 861, AND 1705 MHz

GENERAL

Chapters two through five have dealt with the ambient electromagnetic environment of a hospital produced by fixed location external sources. Contributions to the internal EME in which medical equipment operates within a hospital are also made by sources located indoors. Thus, the goal of this chapter is to examine, in a preliminary way, the EME inside a building due to quasi-mobile internal sources, in an attempt to qualify the EMI hazards medical equipment might be exposed to.

Although signal propagation inside buildings due to internal sources has previously been examined [12-16], these studies have focused on determining and maximizing coverage zones for the future generation of cellular telephones, often referred to as microcellular systems. The following analysis is unique in that it is the first to address the same issue from a different perspective, namely, that of the electromagnetic interference hazard caused by indoor signal propagation due to sources inside a building. With the commonplace existence and growing proliferation of wireless communicators of all types, examining indoor propagation from the perspective of EMI is both timely and necessary.

The three frequencies to be examined here, 433, 861, and 1705 MHz, are representative of current and future operating frequencies of wireless communication systems. Specifically, some walkie-talkies operate around 450 MHz, modern cellular phones use frequency allocations centered around roughly 860 MHz, and microcellular systems are expected to operate between 1.7 and 2.1 GHz.

Indoor propagation at these three frequencies will be examined in a typical, contemporary, multistory urban building, not unlike many hospital buildings. Two types of propagation will be analyzed:

(i) transmitter and receiver on the same floor, propagation along an open path corridor ("same-floor propagation"),

(ii) transmitter and receiver separated by one to nine floors, propagation between floors ("cross-floor propagation").

METHODS

Measurement Location

A McGill University campus building with nine above ground floors and one below ground floor served as the test site. The building, typical of medium height building design, is constructed of reinforced cast and poured concrete. When viewed from the top, the building has a three loop, rectangular cross-section, "doughnut-like" arrangement of (1) rooms, (2) corridors, and (3) core spaces (see figures 6.1-6.3). Offices and lecture rooms are situated in the outside loop around the periphery of the building. More lecture halls are located in the core, or inner loop, of the structure. This area also houses two stairwells, and three elevators at one end. The core is separated from the outer offices and lecture rooms by a rectangular corridor.

The partitioning walls between the outer offices and corridor are of the steel stud and dry-wall type commonly used inside buildings. A combination of plaster and poured reinforced concrete walls separated the corridor from the inner core. Floors were constructed of reinforced concrete.

Figure 6.1 and 6.2 show the top view interior and exterior dimensions of floors three though nine, and the basement level through the second floor, respectively, since the dimensions are not the same. Note that these figures are scaled differently. The floors are spaced vertically an average of 3.4 metres apart.

Measurement Equipment

Three, one watt (30 dBm), continuous wave signals were generated at 433.935 MHz, 861.512 MHz, and 1705 MHz and radiated by a single, triplexer fed, biconical, vertically polarized antenna of approximately 0 dB gain standing 1.14 metres above the ground [12,13]. An identical, vertically polarized, receiving antenna was mounted 0.75 metres above ground on a mobile robot connected by coaxial cable to the receiving unit (monitor, data acquiring equipment) [12,13]. The robot traced out predefined linear paths on each floor where measurements were made at all three frequencies, and position information was recorded. The robot position was stepped in increments of up to three centimetres. The measurements for all three frequencies can be considered simultaneous since the robot was essentially in the same place while each frequency was scanned for twenty milliseconds [13].

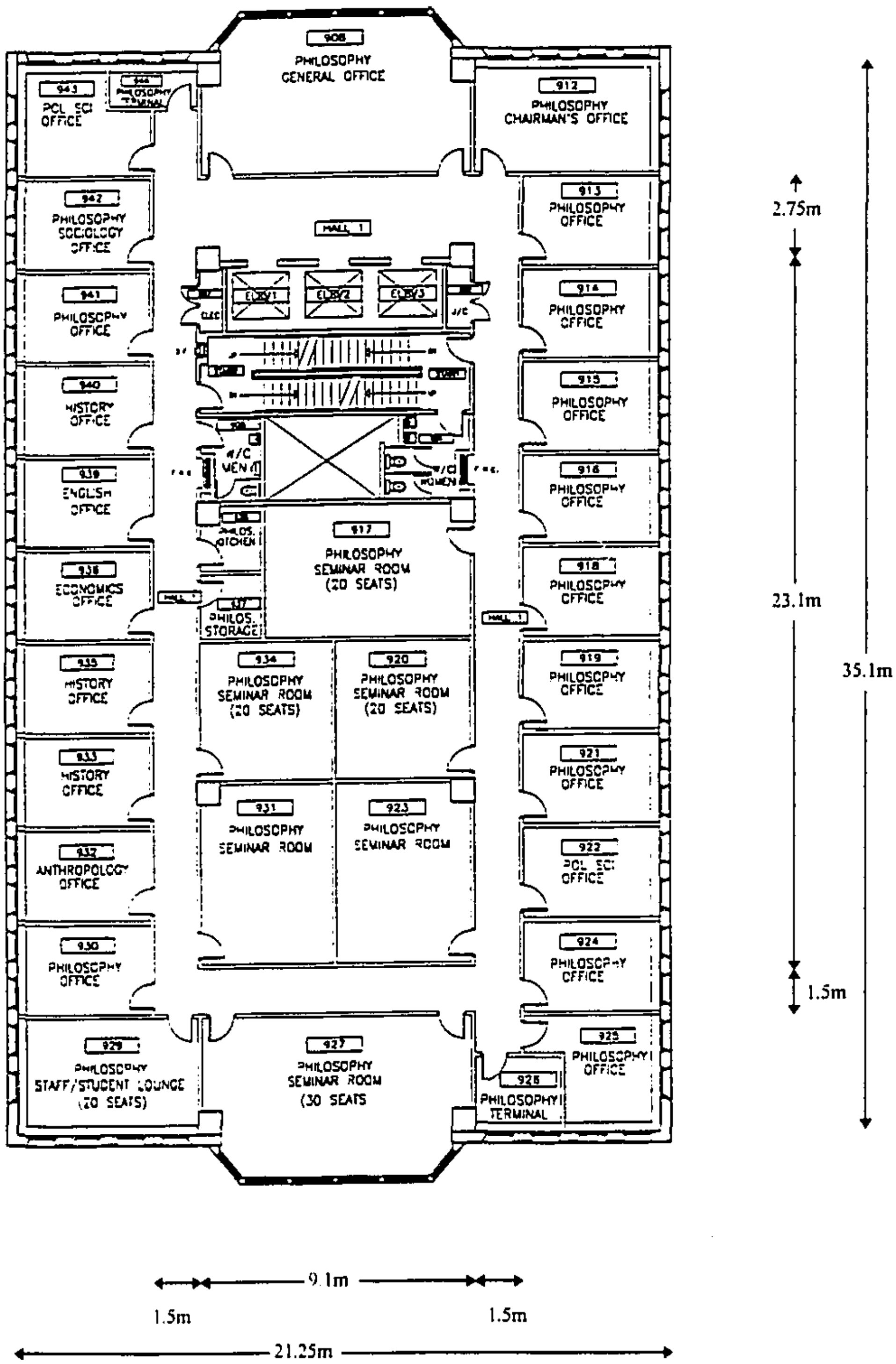

FIGURE 6.1: *Third through ninth floors, top view.*

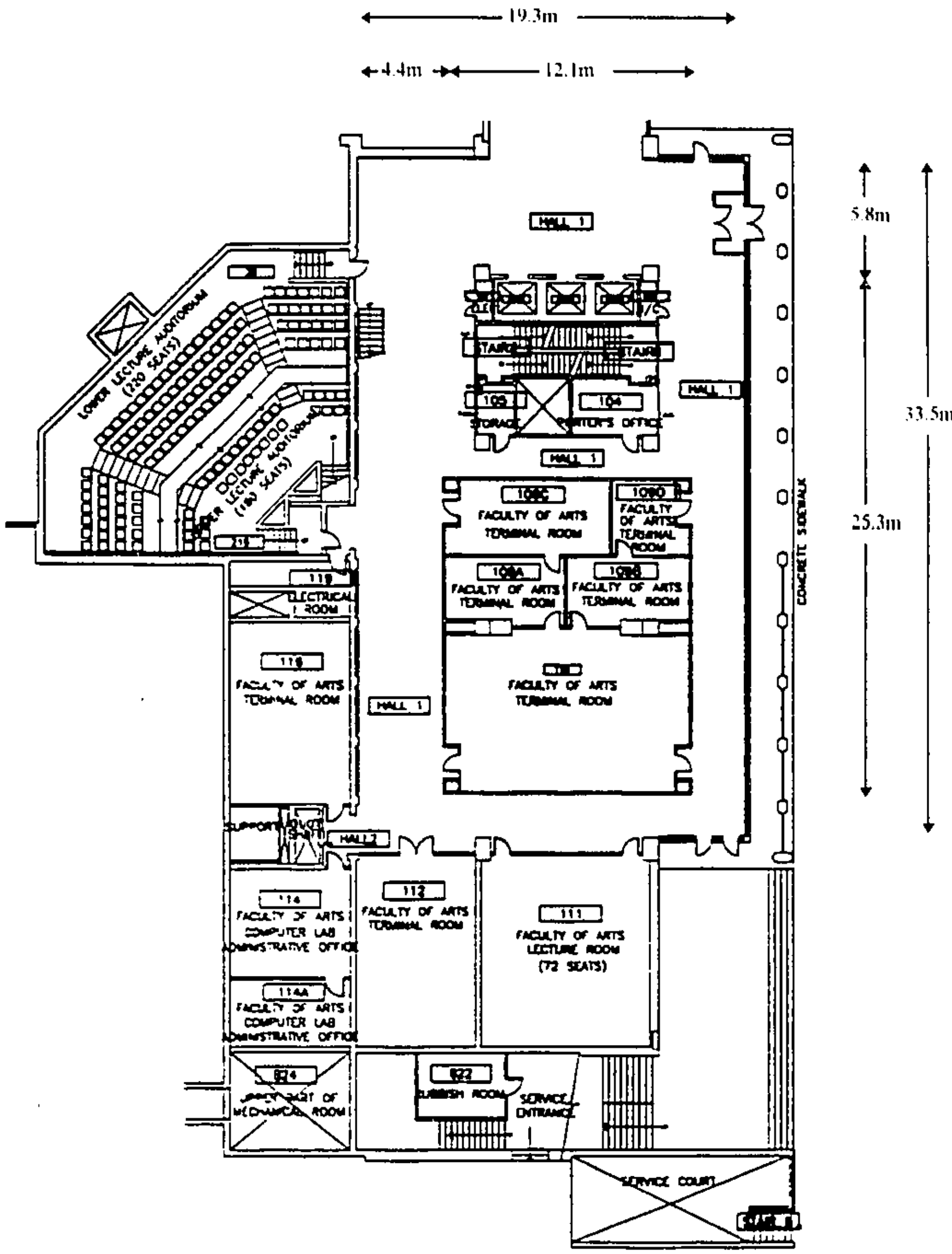

FIGURE 6.2: *Basement through second floors, top view.*

Experimental Procedure

The present analysis utilizes the data collected in 1989 by J. LeBel and P. Melançon, in collaboration with Professor T.J.F. Pavlasek and the Department of Electrical Engineering at McGill University [12]. Measurements in which the transmitter was centrally placed facing the elevators when moved to each subsequent floor are used. The receiver remained on the ninth floor, traveling the closed path around the building in four "segments" between the corners. The corners are labeled one through four for convenience. Correspondingly, the segments traveled by the receiver robot were 1-2, 2-3, 3-4, and 4-1, or their inverse. The labeling scheme is shown in figure 6.3 for clarity and reference. Offices and lecture rooms are shown in gray, the elevators in black, and the corridor in white. The "X" indicates the approximate location of the transmitter on each floor, which is roughly five metres from either corner one or four.

This experimental procedure was engendered by the nature of the measurement equipment described above. The transmitting unit was easily movable from floor to floor. The receiver unit and coaxially connected robot were difficult and awkward to move, thus resulting in the above outlined procedure. This procedure clearly raises the question of reciprocity which will be discussed in the concluding chapter.

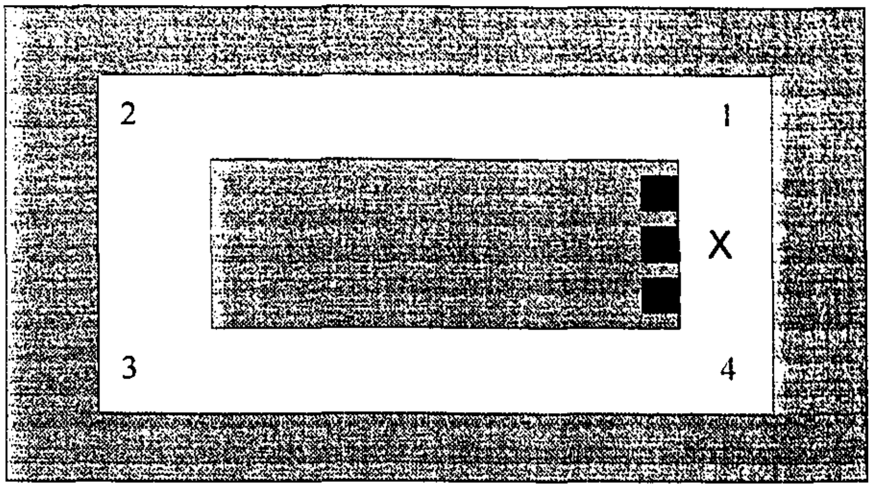

FIGURE 6.3: *Top view of building showing corner and path segment labeling.*

Data Analysis

The signals measured along each corridor segment were smoothed by two passes of a 14 point, rectangular running average 'window' to remove the noisy "spatial fast fading" components. The 'windows' were two, four, or eight wavelengths 'wide' at 433, 861, and 1705 MHz, respectively. Thus, a symmetrical window of about 141 centimetres was used, although other studies have used different window sizes [13,14]. The middle graph in figure 6.4 shows a dashed line indicating the smoothed signal. Note how the filtered data reflects the low frequency components of the original data.

The evaluation of cross-floor propagation characteristics compared the median signal strength for each corridor segment on each floor. A previous study [12] has used one signal value to represent an entire floor, neglecting propagation variances inherent to each corridor segment. This may be misleading in that much of the information about signal behaviour for each segment is lost. It may be of interest to note that certain previous studies have evaluated cross-floor propagation by limiting receiver [12] or transmitter [15] displacement to small areas, whereas the current analysis considers receiver motion over paths ten to twenty-five metres long, depending on the length of the corridor segment. Other investigations have also used results acquired by greater transmitter or receiver displacement [13,14,16].

For every segment on each floor, the median, rather than the mean, value of the raw measured data was used to represent each segment since it tended to remain unaffected by extreme measured values, and so may more appropriately reflect signal behaviour. A survey of some of the literature reveals a dichotomy of opinions. The median value was also used by [14,16], while [13,15] have used mean values.

RESULTS and ANALYSIS

Same-floor Propagation

Figure 6.4 shows examples of the unprocessed measured signal. The graphs shown are for the 1-2 segment on the ninth floor at all three frequencies, when the receiver was located on the ninth floor. The entire survey of the building produces 120 such sets of data. It should be noted that the distance displacement shown on the horizontal axis indicates the distance traveled by the robot receiver, in this case from corner one to corner two, not the separation distance, r, between the transmitter and receiver. Also, y-intercept initial values for best fit lines have been calculated by minimizing the mean square error between the data and an assumed $1/r^2$ power density decay, where again r is the transmitter-receiver separation distance. This will be the convention on all graphs in this section.

The $1/r^2$ regression line indicates that signal strength decays approximately as in free space. This trend is evident for all three frequencies. Each of the three graphs in figure 6.4 indicates the apparent existence of a field perturbation at roughly 1300 centimetres.

The smoothed data presented in figure 6.5 also indicates the existence of such a disturbance (e.g. the large trough from 1200 to 1700 centimetres at 861 MHz). Otherwise, signal levels tended to follow the $1/r^2$ regression line.

Results for segment 4-3 were similar to those of 1-2, presumably due to the symmetry of the building and equipment positioning.

For each of the smoothed curves in figure 6.5, residuals were calculated by subtracting the calculated regression value from the corresponding data point. The mean value of the residuals was calculated, along with the sample standard deviation (SSD). Consequently, for the data in figure 6.5, the mean of the residuals was found to be below 10^{-3} dB, with an SSD of less than 7.2 dB. Note that the mean of the residuals is different from the mean of the data, a quantity which is used later.

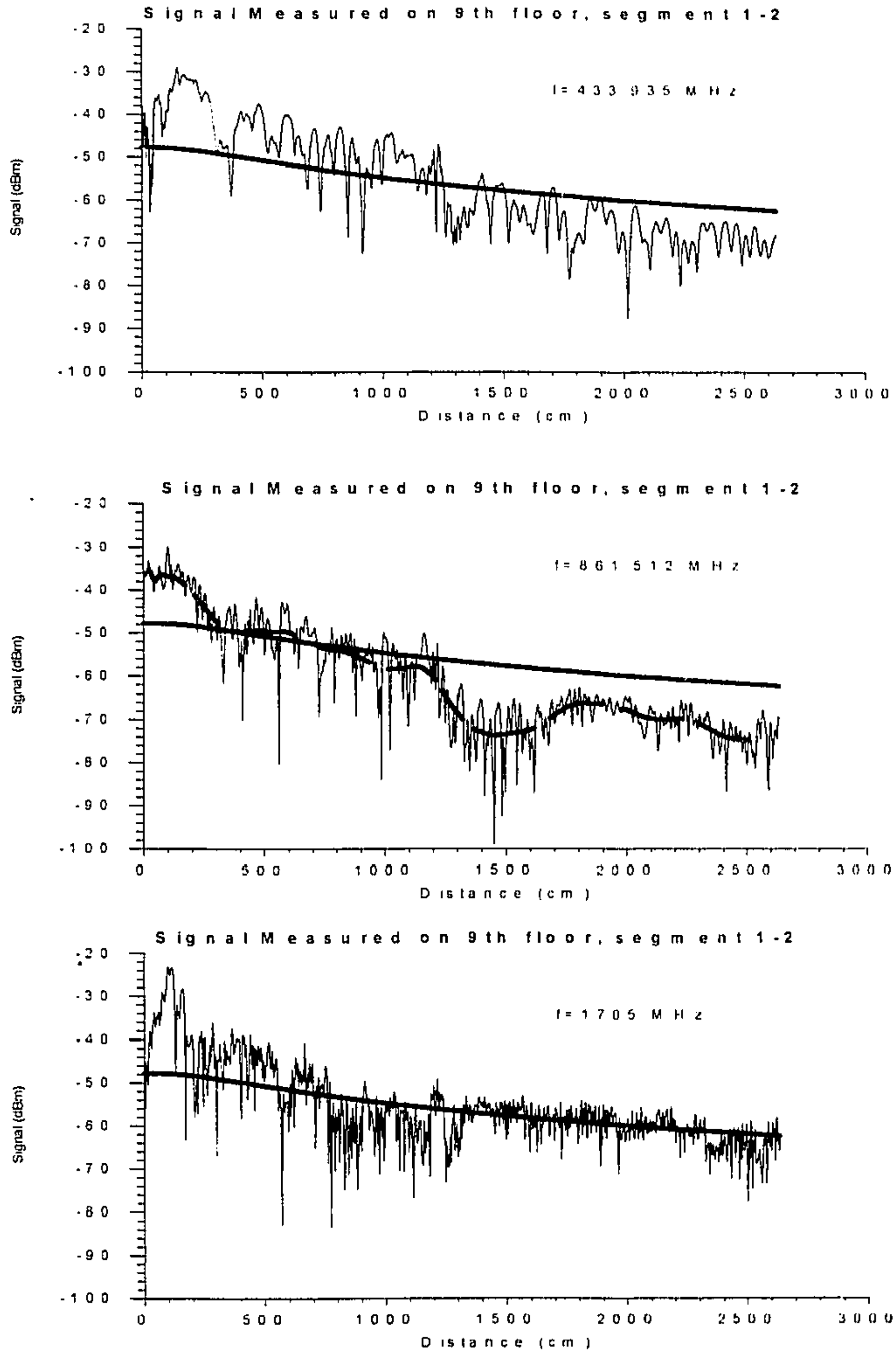

FIGURE 6.4: *Original measured signal with $1/r^2$ regression, segment 1-2, 9th floor, where r is the transmitter-receiver separation distance.*

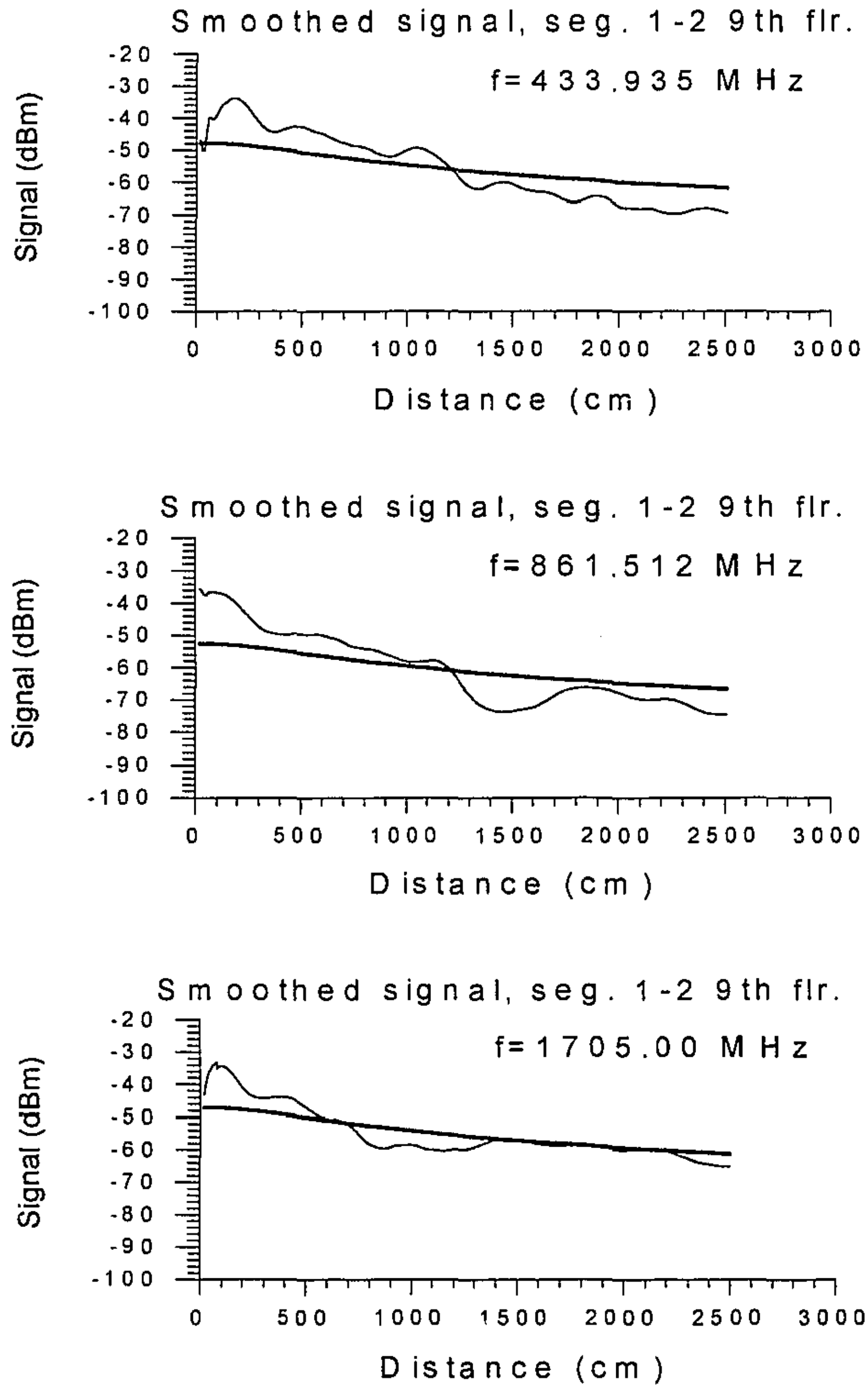

FIGURE 6.5: *Smoothed measured signal with $1/r^2$ regression, segment 1-2, 9th floor, where r is the transmitter-receiver separation distance.*

Figure 6.6 shows the smoothed data collected along segment 2-3 on the ninth floor at the three frequencies. Since the transmitter was roughly five metres from either corner one or four, the straight line distance from corner two (or three) to the transmitter was at most 25.5 meters, or fifty centimetres longer than the perpendicular distance (25m) from the transmitter to segment 2-3. For this reason, the signals in figure 6.6 are referred to their mean, since the difference in path length causes minimal variation in $1/r^2$.

The signal levels along 2-3 are intuitively expected to be relatively constant due to the orientation of segment 2-3 relative to the transmitter. Accordingly, the measurements at 433 and 1705 MHz exhibited oscillation about the mean signal strength, while at 861 MHz, the signal unusually straddled the mean on either side of 500 cm. The sample standard deviation from the mean in each case was less than 2.7 dB, indicating good agreement.

Segment 1-4 is in the immediate vicinity of the transmitting source and the results are shown in figure 6.7. The signal levels measured in this segment are higher than signals in 2-3 due to the proximity of the transmitter and receiver in 1-4. The measured fields are compared to $1/r^2$ regression (short-dashed line) and the mean (long-dashed line) at each frequency. The minimum distance between the transmitter and receiver is assumed to be one metre (passing distance as receiver moves past transmitter). The regression line fits the data increasingly poorly as the frequency of measurement increases. The regression line fit is quite good at 433 MHz, but at 1705

MHz, it is the mean which represents the behaviour of the measured signal more closely. The sample standard deviation (SSD) from the mean of the residuals ($1/r^2$ regression) is about 2.0, 2.9, and 4.4 dB, while the SSD from the mean of the data is roughly 5.8, 2.7, and 1.7 dB at 433, 861 and 1705 MHz, respectively. The mean residual is always less than 10^{-4} dB.

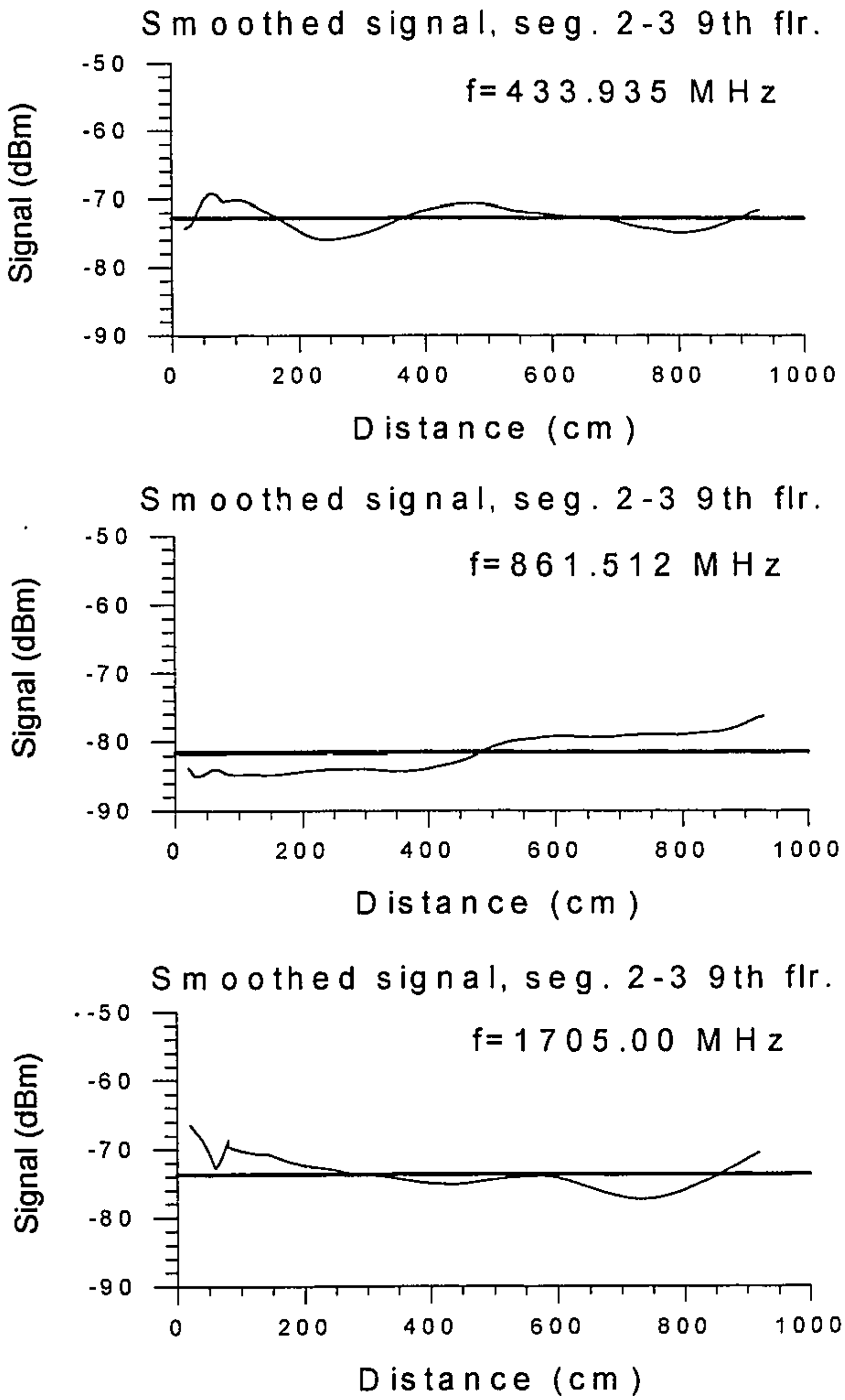

FIGURE 6.6: *Smoothed measured signal referenced to the mean, segment 2-3, 9th floor.*

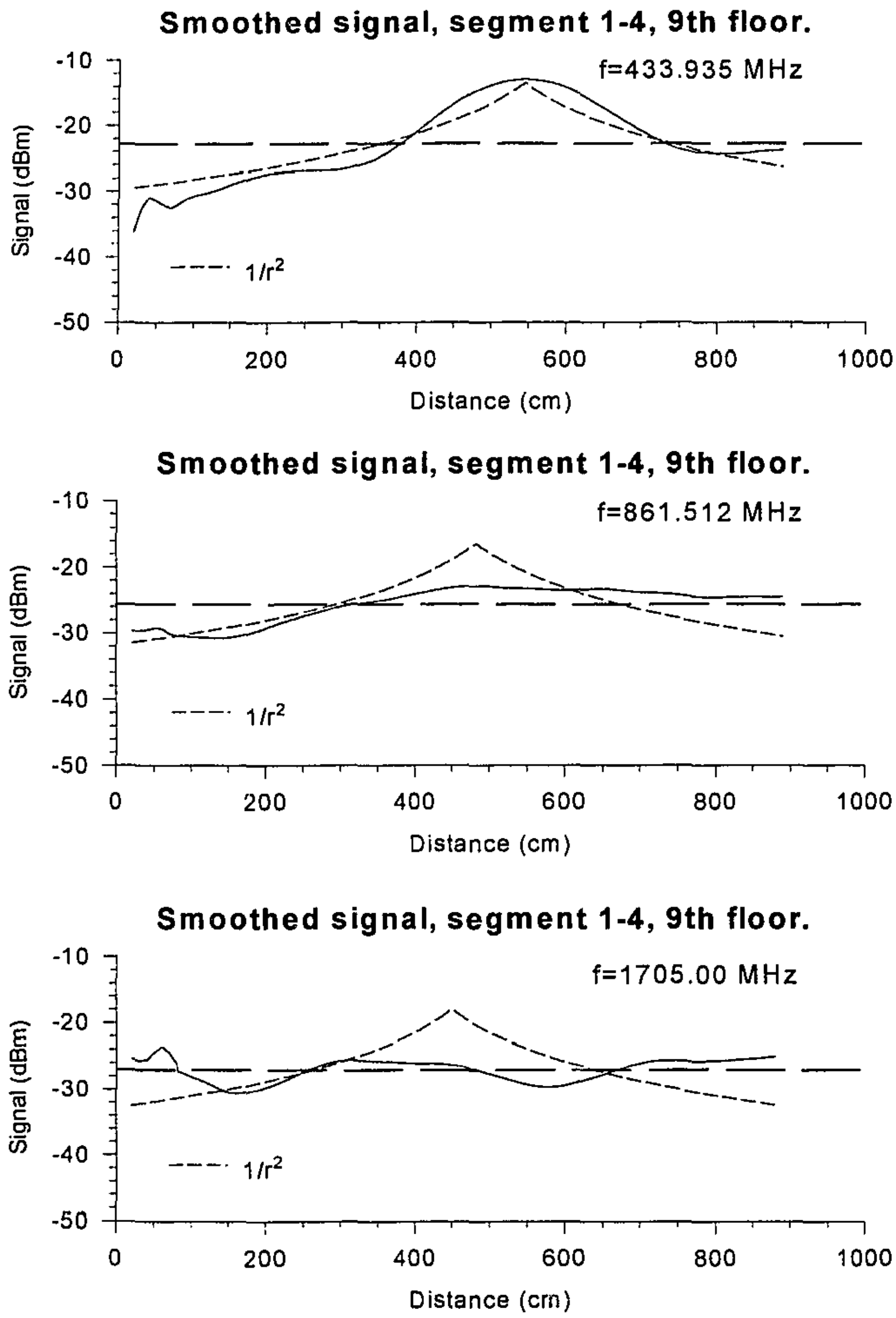

FIGURE 6.7: *Smoothed measured signal referenced to the mean (long dashes) and 1/r² (short dashes), segment 1-4, 9th floor.*

Cross-floor Propagation

Figure 6.8 shows signal propagation between floors at three frequencies for each corridor segment. These figures are plots of the median signal levels for each segment (1-4, 1-2, 2-3, 4-3) on the ten (0-9) floors for each of the three frequencies. The median value was used (see **METHODS**) to characterize the global field strength for each segment on each floor. This form of presentation describes the general behaviour on a given floor, without same-floor horizontal displacement information .

As stated in the **METHODS** section, the receiver unit was located on the top (ninth) floor of the building and the transmitter unit was moved progressively downward, floor by floor. Thus, in all the figures in this section, '0' on the floor separation axis indicates that the transmitter is on the ninth floor, and '1' to '9' represents the placement on successive floors below.

The data in figure 6.8 indicates that signal attenuation tends to increase with increasing frequency. Surprisingly, measured signals at a separation of one floor were usually stronger than same-floor signals (nine of the twelve plotted lines, eight of which occurred for measurements at 433 and 861 MHz). The profiles for segments 1-2 and 4-3 were again similar to each other due to the symmetry of the building and the positioning of the measurement equipment.

In each segment, signal attenuation was initially sharp for the transition between one and two floor separations. Signals decay more gradually for separations of two to eight floors. As the transmitter entered the basement, severe attenuation for a change in separation from eight to nine floors is evident in each segment except 1-4, particularly at 1705 MHz.

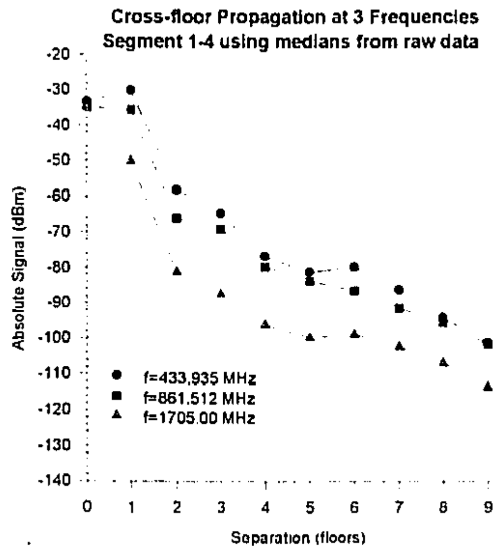

(a) Segment 1-4

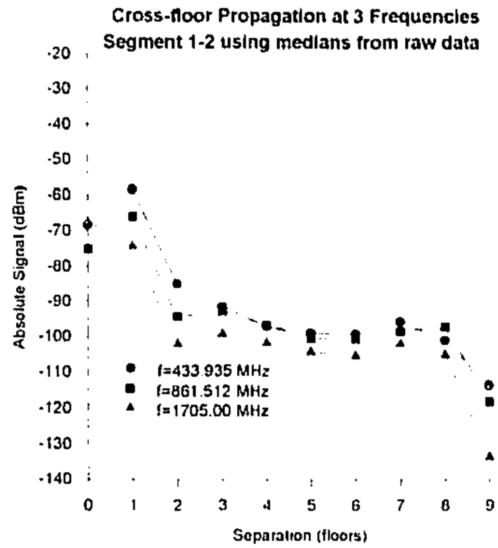

(b) Segment 1-2

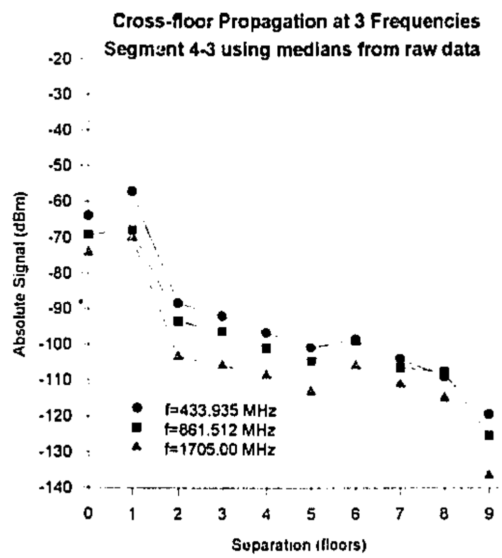

(c) Segment 4-3

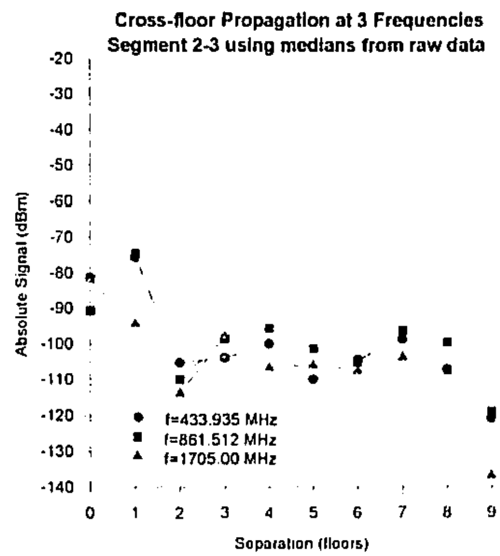

(d) Segment 2-3

FIGURE 6.8: *Cross-floor propagation for each segment at three frequencies.*

Since the transmitter was co-located with the receiver in corridor segment 1-4, measurements made in this segment allowed the examination of signal attenuation caused by floor penetration, unlike segments 1-2, 4-3, and 2-3, where signals must pass through at least one wall and other obstacles.

Thus, the data for segment 1-4 was examined to assess whether a $1/r^2$ power relationship, where r is the vertical transmitter-receiver separation distance in metres, and a floor attenuation constant, FAC, might reasonably describe signal attenuation due to floor penetration. The received signal, P_R, on each floor is expressed by:

P_R [dBm] $= P_{Ro}$ [dBm] $+ 2 * 10 * log_{10}(1/r) + n * FAC$ [dBm/floor] **(6.1)**

where P_{Ro} = received signal, zero separation,

n = number of floors separating transmitter and receiver, and

$r = n$ * 3.4 metres.

Both P_{Ro} and FAC are independent variables determined by minimizing the mean square error in fitting equation (6.1) to the data in figure 6.9. The variable P_{Ro} is used as a convenient way of expressing the initial received signal strength for a transmitter-receiver separation distance approaching zero, without involving antenna gain and radiated power.

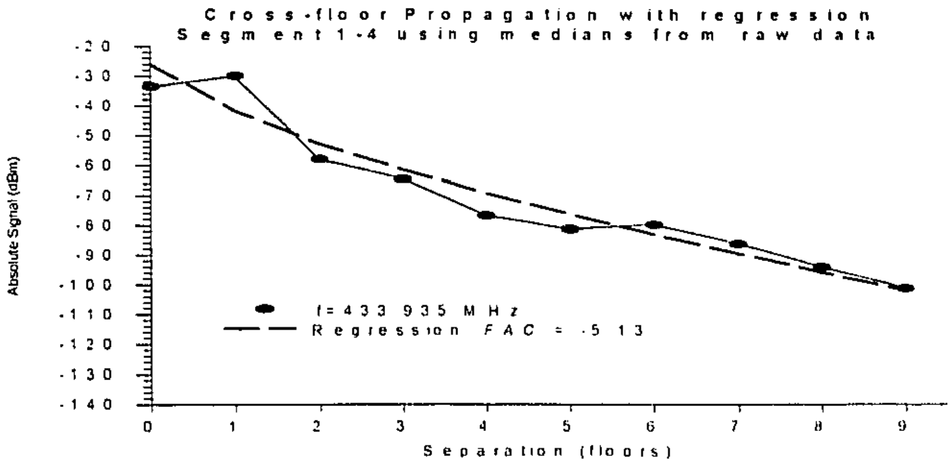

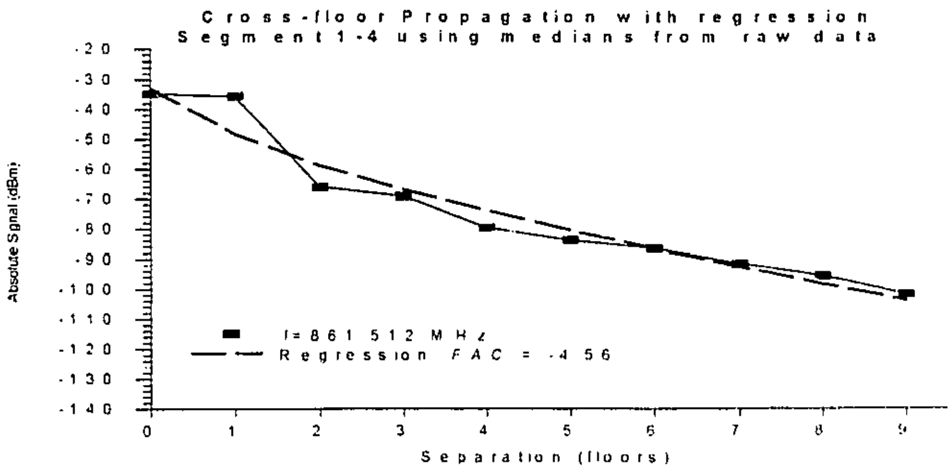

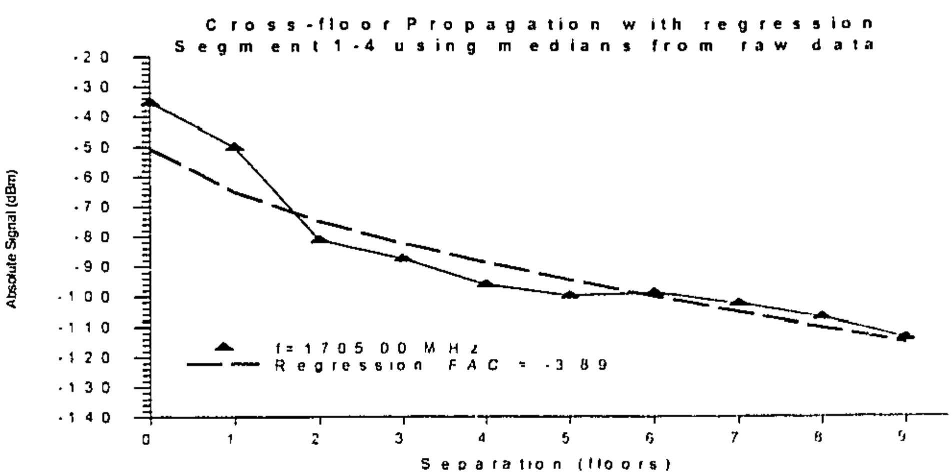

FIGURE 6.9 : *Cross-floor propagation for segment 1-4 with regression.*

Figure 6.9 compares the data of figure 6.8a with signal levels estimated using equation (6.1). As is evident from figure 6.9, equation (6.1) approximates cross-floor propagation in segment 1-4 reasonably well for separations of two or more floors, but poor agreement exists for separations of zero or one floor. The sample standard deviations from the mean of the residuals at 433, 861, and 1705 MHz were 6.1, 5.5, and 8.2 dB, respectively.

An attempt was made to fit equation (6.1) to segments 1-2 and 4-3. The resulting regressions exhibited poorer agreement to the data compared to 1-4. For segment 1-2, *FAC*'s varied from -1.7 to -2.5 dBm/floor, with SSDs from the mean of the residuals of between 7.3 and 8.6 dB. Similarly, *FAC*'s for 4-3 fell between -2.7 and -3.4 dBm/floor, with residual SSDs from 6.4 to 8.7 dB. These results are not surprising since, in these two segments, at least one wall obstructed the direct path from transmitter to receiver.

The most striking characteristic of measurements in segment 2-3 is the almost constant nature of the signals for separations of two to eight floors (region 2). The measured signals in region 2 remain relatively constant, having a sample standard deviation from the mean of about ±4.7 dB at each frequency. The mean values of the data were calculated to be -104.34, -100.99, -106.36 dBm for 433, 861, and 1705 MHz respectively, in region 2. Furthermore, signal levels for a separation of two floors are among the lowest in this region.

An attempt was made to fit equation (6.1) to the data for segment 2-3. The resulting regression lines did not describe the data well, and so are not presented. Sample standard deviations from the mean of the residuals tended to be roughly 9.5 dB with *FAC* values between negative one and two dBm/floor.

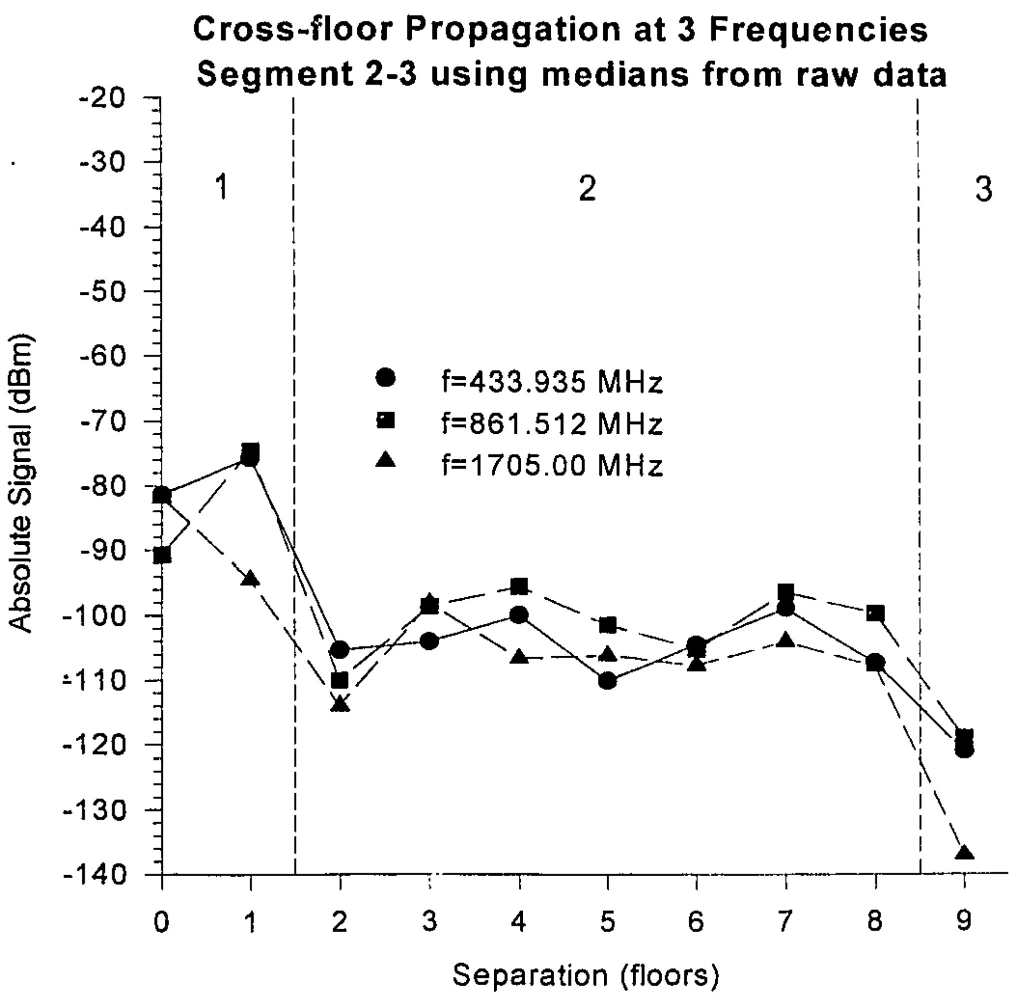

FIGURE 6.10: *Cross-floor propagation for segment 2-3 at three frequencies.*

Discussion

Same-floor Propagation

The reasonable agreement of the data to $1/r^2$ regressions for segments 1-2 and 4-3, and to the mean of the data for segment 2-3, indicates that same-floor propagation inside a building occurred as expected. This conclusion is also supported by signal behaviour in segment 1-4 at 433 MHz, and, to a lesser degree, at 861 MHz. At both frequencies, signals tended to decay as $1/r^2$, although, the 1705 MHz signal in 1-4 tended to be better approximated by the mean of the data.

Cross-floor Propagation

Signal propagation between floors was characterized, generally, by increased attenuation at higher frequencies. Although attenuation at 861 MHz was higher than at 433 MHz, the difference in attenuation from 861 to 1705 MHz was clearly greater.

The signal perturbation observed in figures 6.4-6.5 may have been caused by some physical obstruction or propagation boundary associated with the physical properties of the corridor segment. However, no such structural variation was immediately identifiable from the floor plan.

The floor attenuation constant, FAC, that was used in equation (6.1) is similar to Seidel and Rappaport's floor attenuation factor, FAF [14]. Their FAF is a <u>function</u> of the number of floors separating the transmitter and receiver; thus, a two floor separation has a different FAF than a three floor separation. However, in this analysis, the FAF was assumed, for simplicity, to remain constant from floor-to-floor, hence FAC (in dBm/floor). The results shown in figure 6.9 supported the use of a floor attenuation constant, in addition to $1/r^2$ variation (equation (6.1)), as a feasible approximate description of signal penetration through floors (not including walls).

However, there is some question regarding the significance of FAC values calculated using equation (6.1) since the field at zero floor separation, P_{R_0}, is considered to be an independent variable rather than a value determined from the transmitted signal power, the gain of the transmitting and the receiving antennae, and their separation distance.

The number of walls a signal passes through can be determined by the relative location of the receiver, when stationary, to the transmitter. The mobility of the receiver made it difficult to accurately quantify the number of wall obstructions encountered by signals measured in segments 1-2 and 4-3. Thus, no attempt was made to modify equation (6.1) to include a wall attenuation factor or constant (WAF/WAC). Instead, the need for such a wall attenuation factor was confirmed by observing that the agreement of regressions based on equation (6.1) to the data for these segments was poor. Clearly a more complex regression formulation is necessary to appropriately describe propagation through both floors and walls. One such formulation is presented in [14] based on a wall factor dependent on the number of intervening walls.

The results for segments 1-2, 4-3, and 2-3 (figure 6.8) support the findings of Honcharenko, Bertoni, and Dailing [15] who believe cross-floor propagation in above ground floors is affected by, and eventually dominated by, creepy waves which escape the confines of the building through windows, propagate down the outside walls, and re-enter via windows on lower floors. Accordingly, attenuation between the first above-ground floor and the first below-ground floor was higher than for attenuation between most above-ground floors.

In segment 1-4, however, the general agreement between the regression lines and the data fails to corroborate the creepy wave hypothesis of Honcharenko *et al* [15] in that no significant increase in attenuation occurs when the transmitter is moved to the basement from the first above-ground floor. However, the position of the transmitter relative to the receiver, for this segment (e.g. vertically in line, no wall obstructions), may have resulted in signal levels that were "too high" to allow creepy waves to become dominant, and therefore evident.

A highly significant result was the observation that signal levels remained quasi-constant for separations of two to eight floors in segment 2-3 (figure 6.10). For example, it was found that signals seven metres (two floors) away from the transmitter were roughly equal to, or lower than, signals twenty-seven metres (eight floors) away. It can therefore be concluded that signal behaviour in region two of figure 6.10 is not accurately described by a $1/r^2$ relationship, since signal levels remained relatively constant, independent of transmitter-receiver separation distance.

This result indicates the need for a more extended consideration of the problem of EM wave propagation inside buildings, as well as further studies to establish the generality of these results. The impact of these results is considerable, particularly in view of the increased interest and expected growth of personal communication services (e.g. wireless local area networks, "pico-" cellular systems).

Chapter 7

SUMMARY AND CONCLUSIONS

GENERAL SUMMARY

The research reported in this thesis is one component of a broader research program, currently under way, to consider electromagnetic interference in hospitals which affects the reliability and dependability of electronic medical equipment operation. The specific concerns of the work in this thesis have been:

(1) To consider the electromagnetic environment outside and inside hospitals, due to fixed, external transmitters operating in the 30 - 1000 MHz range and to develop simple computational methodologies for predicting such fields outside hospitals;

(2) To analyze the propagation characteristics inside buildings due to internal sources operating at 433, 861, and 1705 MHz.

PART ONE

Summary

This part of the thesis, chapters two through five, assessed, by measurement and prediction, the outside and inside EMEs at a hospital due to fixed, external sources. The focus was on radiators between 30 - 1000 MHz, and particularly emissions in the FM radio, television, and cellular telephone base station bands, since these comprise the major radiating sources in this spectral range. A principal objective was to develop computational techniques, based on free-space propagation modeling, which would allow the prediction of outside fields due to external sources. These techniques should be simple, rapidly applicable, and meaningful, thereby reducing the necessity for complex, costly, and time consuming measurements. Such techniques need not acquire the complex forms of telecommunication systems' point-to-point propagation modeling since only estimates of the order of magnitude of the potential EME threats are necessary. Yet, such estimates are needed in large numbers for many different sites to characterize these threats in hospitals.

Measurements of the outside and inside EMEs at five hospitals were presented in chapter two.

Chapters three, four, and five described the various methods which have been evolved and evaluated in trying to fulfill the above requirements. As described in these chapters, the four methods examined were designated the LOS A, the LOS B, the Hybrid A, and the Hybrid B methods.

It should furthermore be observed that the four prediction methods exhibit varying degrees of success for the five sites which were evaluated. The choice of method used to make field predictions, for a close estimate, is to a degree a heuristic process involving judgment and experience on the part of the user. Thus, while the objective of evolving suitable prediction methods has been achieved, it is evident, nevertheless, that measurements cannot be dispensed with entirely.

Conclusions

(1) Measured field levels were at most 2 dB higher than the U.S. FDA standard, ranging from 40 - 135 dBμV/m (10^{-4} - 5.62 V/m) for combined outside and inside results.

(2) The Hybrid B method predicted field levels closest to the measured data (within 10 dB), while still remaining relatively simple and quick to use. If a close estimate of field levels is desired, the Hybrid B should be used (figures 5.1-5.2);

(3) The LOS A prediction method provides a worst-case estimate of fields at a hospital by predicting field levels higher than the measured fields (within 20 dB). It is also the simplest of the four methods considered (figures 5.1-5.2).

PART TWO

Summary

The second part of the thesis, chapter six, dealt with the analysis of EM wave propagation, due to internal sources, inside a building similar to a typical hospital. The analysis was based on measurements made at 433, 861, and 1705 MHz, which are some of the frequencies that are, or will be used for personal communication services, ranging from wireless local area networks for computers to cellular telephone systems.

Conclusions

(1) Same-floor propagation was essentially well approximated by $1/r^2$ signal power variation (figures 6.4-6.7);

(2) Cross-floor propagation paths which were not obstructed by walls (segment 1-4, figure 6.9) indicated a general tendency for signal powers to decay as $1/r^2$;

(3) Cross-floor paths where multiple floors and walls were traversed showed that signal strengths remained essentially constant, regardless of transmitter-receiver separation distance (segment 2-3, figure 6.10);

(4) Signal attenuation between floors tended to increase with increasing frequency;

(5) Signal levels measured for a single floor separation were higher than same-floor signal levels (figure 6.8);

(6) The findings, based on measurements, supported the computational "creepy wave" theory for cross-floor propagation, presented by Honcharenko *et al* [15]. This was emphasized by the different behaviour above-ground, where a creepy wave might be expected, as compared to the below-ground behaviour.

Note that further investigation is required to establish the generality of these results.

AREAS OF FUTURE WORK

In dividing the 30 - 1000 MHz spectrum into six distinct active bands (chapter two, figure 2.1, table 2.2), it became clear that little was known about the failure modes of medical equipment. Medical equipment itself is broadband since it has not been designed to be frequency selective, and as such may be susceptible at one (or several) individual frequencies.

A corollary is the EMI effect on electronic medical equipment when the equipment is subject to many simultaneously active radiating sources, either over a wide spectral range, or as a cluster of sources within a particular band, resulting in an EME with integrated power density. This, in turn, leads to the question of whether meaningful susceptibility standards for medical equipment should be defined for power emissions at individual frequencies, or over frequency bands with many simultaneously active radiating sources.

The issue of the failure modes of electronic medical equipment subject to broadband radiation poses a challenging problem. It is an area where the literature is sparse at present, and represents a significant problem which merits study, experimentation, and analysis.

Signal penetration into a building due to external sources, though not addressed in the thesis, is the link that inextricably relates the outside EME at a hospital to the inside EME. Although the literature shows this issue has been addressed, it nevertheless is an important complementary consideration which requires further investigation.

It was frequently observed (figure 6.8) that the signal measured on the eighth floor exceeded the signal measured on the ninth floor, indicating a gain, rather than a loss, for a separation of one floor. This raises significant questions regarding the process of propagation inside a building.

Reciprocity refers to the relative placement and displacement of the transmitting and receiving equipment in performing cross-floor measurements. Recall that the experimental procedure was dictated by the ease with which the experimental equipment could be moved between floors. Due to the bulky, awkward nature of the receiving unit, it was decided to displace the transmitter unit downward from one floor to the next. There is some question as to whether this configuration is equivalent to stationing the transmitter unit on the top floor and displacing the receiver unit progressively to the lower floors, which, disregarding the physical dimensions of the test equipment, may seem a more intuitive configuration. In this and previous studies [12-16], the two measurement configurations used have been considered to be identical by invocation of the reciprocity theorem. The issue of reciprocity under indoor propagation conditions, however, poses an interesting consideration which merits further investigation.

APPENDIX A

PREDICTING THE ELECTROMAGNETIC ENVIRONMENT AT ANY LOCATION USING GRAPHICAL LINE-OF-SIGHT (LOS) METHODS

CHART 1 : PURPOSE

Chart A.1 on page A-3 is designed to be used to calculate the approximate electric field (at any location) arising from nearby transmitters. The calculation technique is based on a free-space line-of-sight propagation method which is frequency independent (LOS A). The requirements are a knowledge of the three-dimensional distance between the transmitter and survey location, and the effective isotropic radiated power (EIRP) of the transmitter. According to a comparison at five outdoor sites, the field strengths predicted tended to be, on average, 20 dB higher than the actual fields measured. Propagation conditions tended *not* to be true LOS. Conditions where the transmitter was in direct view from the survey site indicated predictions were an average of 10 dB higher than measured fields.

This chart can also be used to find resultant electric field equivalencies between mobile, low power radiators at short distances, and fixed, high power radiators at many kilometre distances (see **Example** below).

Note: The resultant fields are always assumed to be *far-field*. It is the user's responsibility to ensure that far-field conditions exist, particularly in dealing with small separation distances.

CHART 1 : USAGE

To use chart A.1, find the transmitter effective radiated power on one of the left-hand axes, indicated as EIRP (effective isotropic radiated power), either in dBW or Watts (the transmitter is assumed to be an isotropic radiator, hence EIRP). If the radiated power does not correspond to one of the pre-plotted lines (100W, etc.), then interpolation between the lines is necessary, and simple with the aid of a ruler. Next, travel the necessary separation distance along this sloped line, at which point the resultant power or electric field can be read off using the right-hand axes.

Example: A fixed transmitter has an effective isotropic radiated power of 50 dBW. Predict the electric field at a site one kilometre from the transmitter.

Solution: Using the two left-hand axes of chart A.1, 50 dBW is equivalently a radiated power of 10^5 W (or 100 kW). Find the sloped line marked 100 kW, and follow it to a separation distance of 1000 metres. Reading the resultant value of the field from any of the right-hand axes gives, at the site, a power of 8×10^{-3} W/m^2, or a field of 2.45 V_{rms}/m ~ 128 dBμV/m.

Note that the field at the site is roughly equivalent to a (mobile) source radiating 0. 1 W (100mW, or -10 dBW) at a distance of one metre.

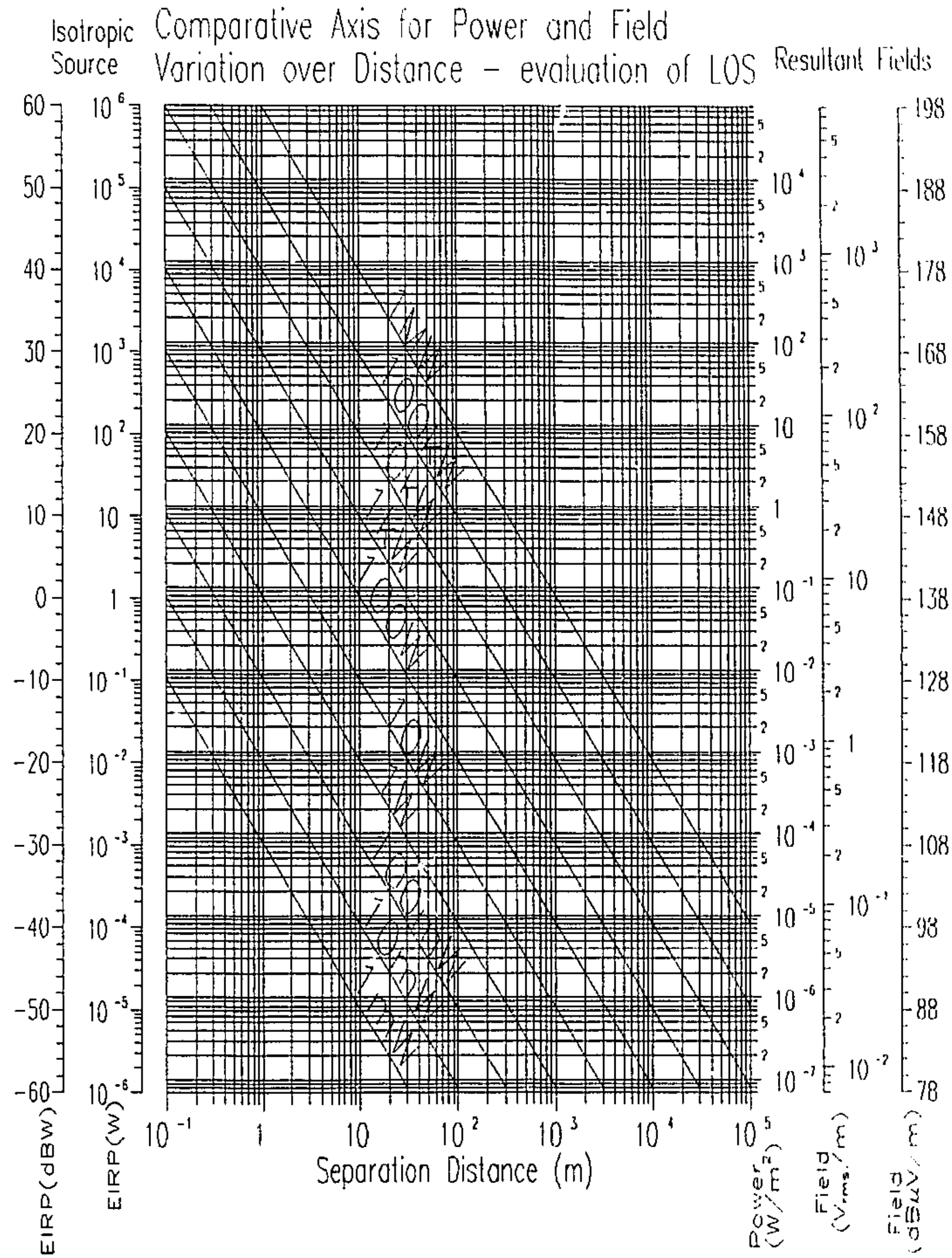

CHART A.1: *Graphical method of predicting fields using an LOS A method.*

CHART 2 : PURPOSE

Chart A.2 on page A-6 is designed to be used to calculate the approximate electric field (at any location) arising from nearby transmitters. The calculation technique is based on a free-space line-of-sight propagation method which is frequency dependent (LOS B). The requirements are: a knowledge of the three-dimensional distance between the transmitter and survey location; the effective isotropic radiated power (EIRP) of the transmitter; and the transmission frequency. According to a comparison at five outdoor sites, the field strengths predicted tended to be, on average, 15 dB higher than the actual fields measured. Propagation conditions tended *not* to be true LOS.

Note : The resultant fields are always assumed to be *far-field*. It is the user's responsibility to ensure that far-field conditions exist, particularly in dealing with small separation distances.

CHART 2 : USAGE

The Frequency Component graph is used to determine the frequency component, A. Locate the transmission frequency on the horizontal axis. Find the power (dBW) contribution along the plotted line corresponding to this frequency. Subtract this value, A, from the radiated power of the transmitter (EIRP), in dBW.

To determine the distance component, B, use the second graph labeled Distance Component. On the horizontal axis, locate the separation distance corresponding to the site under observation. Next, read off the power contribution along the plotted line at this separation distance. This is the distance component, B. Subtract B from the difference obtained using the Frequency Component graph. The full formula is shown on the chart as

$P_{site}(dBW) = EIRP(dBW) - A - B.$

The conversion axes below the formula serve to translate power (dBW) to power (W) or electric field (V_{rms}/m or dBμV/m). A simple example may be useful.

Example: A transmitter irradiates a site one kilometre away with a signal of 50 dBW at a frequency of 100 MHz. Predict the field at the site.

Solution: Using the Frequency Component graph, A = 56 dBW. Similarly, using the Distance Component graph, B = 17 dBW.

Therefore, $P_{site}(dBW) = 50 - 56 - 17$ dBW = -23 dBW, or E_{site} = 126 dBμV/m.

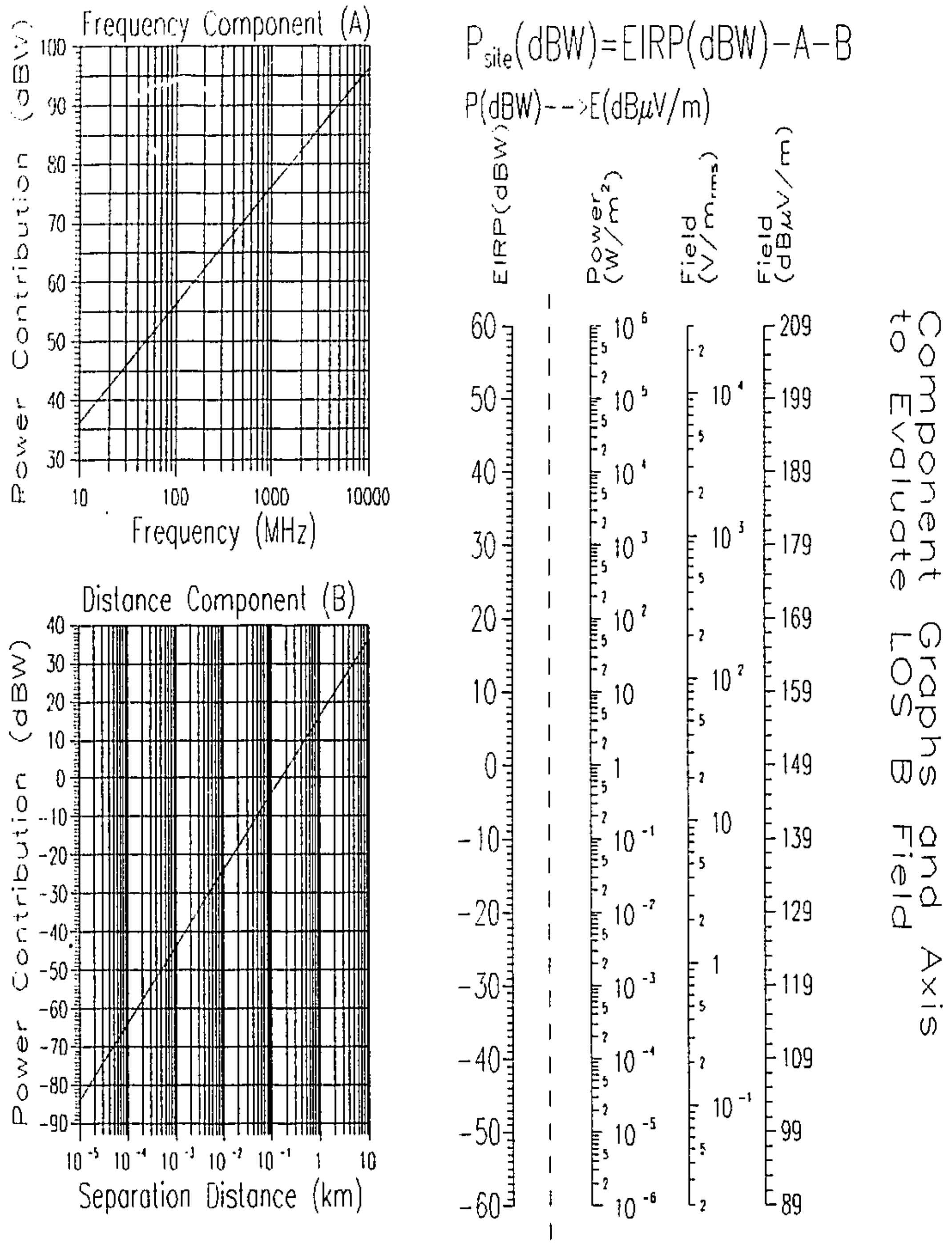

CHART A.2: *Graphical method of predicting fields using an LOS B method*

APPENDIX B

ABBREVIATIONS

EM	Electromagnetic
EMC	Electromagnetic compatibility
EME	Electromagnetic environment
EMF	Electromagnetic field
EMI	Electromagnetic interference
ESD	Electrostatic discharge
EIRP	Effective isotropic radiated power
FAC	Floor attenuation constant
FAF	Floor attenuation factor
FDA	Food and Drug Administration (U.S.)
LOS	Line-of-sight
RF	Radio frequency
SSD	Sample standard deviation
UGTD	Uniform Geometric Theory of Diffraction
WAC	Wall attenuation constant
WAF	Wall attenuation factor

REFERENCES

[1] Silberberg J L. *Performance Degradation of Electronic Medical Devices due to Electromagnetic Interference*. Compliance Eng 10: 25-39. Fall, 1993.

[2] Segal B, Pavlasek T, Rétfalvi S, Silberberg J L. *Medical Device Int: Problems & Prevention*, TeleMedicine Canada Teleconference, Montreal, Oct. 22, 1993.

[3] Boisvert P, Segal B, Pavlasek T, Rétfalvi S, Sebe A, Caron P. *Preliminary Survey of the Electromagnetic Interference Environment in Metropolitan Hospitals*. IEEE Int Symp Electromagnetic Compatibility, Cherry Hill, N.J., June 1991.

[4] Segal B, Boisvert P, Rétfalvi S, Pavlasek T, Sebe A, Caron P. *Identification of hospitals having electromagnetic environments that might cause medical device malfunction*. Proc Can Med Biol Eng Soc Conf, June 1992, p. 244-5.

[5] FDA MDS 201 00041979, *Electromagnetic Compatibility Standard for Medical Devices*, published by the US Dept. of Health, Education and Welfare, Food and Drug Administration, Bureau of Medical Devices.

[6] Vlach P, Segal B, Pavlasek T, Boisvert P, Rétfalvi S, Sebe A, Caron P, Zafar A, Massaad M. *Prediction of Maximal Electromagnetic Fields Outside Hospitals*. Proc Can Med Biol Eng Soc Conf, May 1994, p. 22-3.

[7] Boisvert P. *The Ambient Electromagnetic Environment in Metropolitan Hospitals*. Masters Thesis, Dept. of Electrical Engineering, McGill University, 1991.

[8] Koyoumjian R G, Pathak P H. *A Uniform Geometrical Theory of Diffraction for an Edge in a Perfectly Conducting Surface*. Proc. IEEE, Vol. 62, No. 11, November 1974, p. 1448-61.

[9] Skomal E N, Smith A A. <u>Measuring the Radio Frequency Environment</u>. New York: Von Nostrand Reinhold Company Inc. , 1985.

[10] Stutzman W L, Thiele G A. <u>Antenna Theory and Design</u>. New York: John Wiley & Sons Inc., 1981.

[11] McCall R B. <u>Fundamental Statistics for Behavioral Sciences</u>. 4th ed. San Diego: Harcourt Brace Jovanovich Inc., 1986.

[12] LeBel J, Melançon P. *The Development of a Comprehensive Indoor Propagation Model.* IEEE Symp on Personal, Indoor and Mobile Radio Communications, King's College, London, U.K., 23-25 September 1991.

[13] Melançon P. *Report on Propagation Inside an Empty and Furnished Building at 433, 861 and 1705 MHz.* Proc 15th Biennial Symp on Comm, Kingston, Canada, June 3-6, 1990.

[14] Seidel S Y, Rappaport T S. *914 MHz path Loss Prediction Models for Indoor Wireless Communications in Multifloored Buildings.* IEEE Trans on A & P, Vol. 40, No. 2, February 1992, p. 207-17.

[15] Honcharenko W, Bertoni H L, Dailing J. *Mechanisms Governing Propagation Between Different Floors in Buildings.* IEEE Trans on A & P, Vol. 41, No. 6, June 1993, p. 787-90.

[16] Arnold H W, Murray R R, Cox D C. *815 MHz Radio Attenuation Measured Within Two Commercial Buildings.* IEEE Trans. on A & P, Vol. 37, No. 10, October 1989, p. 1335-39.

BIBLIOGRAPHY

Graphical Analysis

Chambers J M, Cleveland W S, Kleiner B, Tukey P A. Graphical Methods for Data Analysis. New Jersey: Bell Telephone Laboratories Inc., 1983.

Uniform Theory of Diffraction Analysis

Deygout J. *Correction factor for multiple knife-edge diffraction.* IEEE Trans. on A & P, Vol. 39, No. 8, Aug. 1991, p. 1256-8.

Herrmann G F. *Numerical Computation of Diffraction Coefficients.* IEEE Trans. on A & P, Vol. AP-35, No. 1, Jan. 1987.

Jakibsen K R. *An Alternative Diffraction Coefficient for the Wedge.* IEEE Trans. on Antennas & Propagation, Vol. AP-32, No. 2, Feb. 1984.

Jiang K, Maclean T S M, Wu Z. *Comparison of G.T.D. with Compensation Theorem for Finite Size Knife Edges.* IEE Seventh Int Conf on A & P, ICAP 91, Vol. 1, p. 221-5.

Lee Shung-Wu, Deschamps, G A. *A Uniform Asymptotic Theory of Electromagnetic Diffraction by a Curved Wedge.* IEEE Trans. on A&P, Vol. AP-24, Jan. 1976, p.25-34.

Michaeli A. *A Uniform GTD Solution for the Far-Field Scattering by Polygonal Cylinders and Strips.* IEEE Trans. on A & P, Vol. AP-35, No. 8, Aug. 1987.

Rektorys Karl ed. Survey of Applicable Mathematics. London: Iliffe Books Ltd., 1969, p. 688-689.

Ross R A. *Scattering by a Wedge with Rounded Edge.* IEEE Trans. on A & P, Vol. AP-19, No. 4, July 1971.

RADIOWAVE PROPAGATION

Banik T. *Spatial fading Characteristics of VHF Broadcast Signals in an Urban Environment.* Masters Thesis, Dept. of Electrical Engineering, McGill University, July 1988.

Bertoni H L, Maciel L R. *Theoretical prediction of slow fading statistics in urban environments.* IEEE Proc. 1st Int Conf on Universal Personal Communications, ICUPC '92, 1992.

Damasso E, Paraboni A, Protto F. *Indoor propagation measurements application to mobile channel modelling.* IEE Eighth Int Conf on A & P, Vol. 1, p. 146-9.

Larsen D M, Notestine P L. *MSRFM-a prediction tool for radio system design.* 40th IEEE Vehicular Tech Conf. On the Move in the 90's, p. 378-83.

Maciel L R, Bertoni H L, Xia H H. *Unified Approach to Prediction of Propagation Over Buildings for all Ranges of Base Station Antenna Height.* IEEE Trans. on Vehicular Tech, Vol. 42, No. 1, Feb 1993, p. 41.

McGrane A R. *A Microwave Propagation Prediction Tool, MPT, and its performance in practice.* IEE Colloquium on 'Diffraction Propagation Modelling Techniques Embracing Surface Feature Data', No. 157.

Mizuike T, Watanabe F, Kimura T, Minamisono K, Kishi Y. *Computer-aided modelling for interference analysis in urban areas.* IEEE Global Telecom Conf, GLOBECOM '92, Vol. 3, p. 1858-64.

Saunders S R, Bonar F R. *A propagation model for slow fading in urban mobile radio systems.* IEE Seventh Int Conf on A & P, ICAP 91, Vol. 1, p. 160-3.

Sharples P A, Mehler M J. *An integrated terrain and urban diffraction model for system planning.* IEE Seventh Int Conf on A & P, ICAP 91, Vol. 2, p. 808-11.

Sharples P A, Mehler M J. *Propagation modelling in microcellular environments.* IEE Eighth Int Conf on A & P, Vol. 1, p. 68-71.

Xia H H, Bertoni H L, Maciel L R, Lindsay-Stewart A, Rowe R. *Radio Propagation Characteristics for Line-of-Sight Microcellular and Personal Communications.* IEEE Trans. on A & P, Vol. 41, No. 10, Oct. 1993, p. 1439-47.

Xia H H, Bertoni H L, Maciel L R, Rowe R, Lindsay-Stewart A, Grindstaff L. *Urban and suburban microcellular propagation.* IEEE Proc. 1st Int Conf on Universal Personal Communications, ICUPC '92, 1992.

GENERAL

Balanis C A. Antenna Theory Analysis and Design. New York: Harper & Row, Publishers, Inc., 1982.

Johnk C T A. Engineering Electromagnetic Fields and Waves, 2nd ed. New York: John Wiley & Sons, Inc., 1988.